This is a post-print (peer-reviewed, corrected) version of: Omosanya, K.O., Harishidayat, D., Marheni, L., Johansen, S.E., Felix, M., Abrahamson, P. (2016) Recurrent mass-wasting in the Sørvestsnaget Basin Southwestern Barents Sea: A test of multiple hypotheses. Marine Geology, Volume 376, 1 June 2016, Pages 175-193. https://doi.org/10.1016/j.margeo.2016.03.003.

Recurrent mass-wasting in the Sørvestsnaget Basin Southwestern Barents Sea: A test of multiple hypotheses

Omosanya, K.O.[1]*, Harishidayat, D[1], Marheni, L.[2], Johansen, S.E.[1], Felix, M.[2], Abrahamson, P[3]

[1] Department of Petroleum Engineering and Applied Geophysics
[2]Department of Geology and Mineral Resources Engineering
Norwegian University of Science and Technology
Trondheim

[3]MultiClient Geophysical, Stasjonsveien 18 1396 Billingstad, Norway

Corresponding author: kamaldeen.o.omosanya@ntnu.no

Abstract

Mass-wasting on the NE Atlantic margin is generally attributed to Cenozoic glaciations. Using high-quality 2D seismic datasets and two exploration wells, this study investigates the types and driving mechanisms of mass-wasting in the Sørvestsnaget Basin, Southwestern Barents Sea. The methods include seismic interpretation of shelf margin clinoforms, mass-transport deposits (MTDs), submarine channels and v-shaped canyons. The shelf-edge trajectory provided information about sea-level conditions, paleo-sediment routes, and dispersal patterns during the evolution of the basin. In terms of the internal geometry of reflectors, the major depositional units in this work are five sedimentary packages (P1 to P5) characterised by distinct southwest dipping shelf margin clinoforms. The seven MTDs here discussed have Late Miocene to Pleistocene ages. Miocene and Early Pliocene MTDs in the basin demonstrate a tendency for initial translation through canyons and channels. The youngest MTDs are composed of glaciogenic sediments remobilized by ice streams during large-scale Neogene and Quaternary glaciations. This work shows that mass-wasting has been a recurrent and inherent process in the Sørvestsnaget Basin from the Miocene until recent times. The main triggering

mechanisms for slope failure in the basin are increased pore pressure from sea-level fall and high sedimentation rate. Mass-wasting in the study area occurred through progressive, retrogressive and coherent downslope failures.

Keywords: Barents Sea, mass-wasting, Sørvestsnaget, glaciations, erosion, recurrence.

1. Introduction

Mass-wasting is a geological process that involves the re-sedimentation of originally deposited unconsolidated sediments under the influence of gravity (Posamentier and Kolla, 2003; Varnes, 1978). Mass-wasting occurs on all kinds of continental margin settings, from passive to active and in glacial to equatorial regions (Laberg et al., 2000; Masson et al., 2002; Piper et al., 1999; Solheim et al., 2005; Trincardi and Argnani, 1990; Urgeles et al., 2007). Mass-wasting represents the fundamental process of transporting sediment to deep-water environmental and can generate geohazards such as tsunamis, and widespread damage of subsea installations (Frey Martinez et al., 2005; Gee and Gawthorpe, 2006; Richardson et al., 2011). Evaluating the recurrence of mass-wasting or sediment failure is thus important to understand the evolution of continental margins (Minisini and Trincardi, 2009; Mulder and Cochonant, 1996).

The region spanning the Norwegian Sea, Barents Sea and the Svalbard islands represents a repository of formerly glaciated margins, on which some of the largest submarine landslides in the world have been documented (e.g., Storegga Slide, Andøya Slide, Afen Slide, Tampen Slide, Bjørnøya Slide, Møre Slide, Bjønørya Mouth Fan, to mention a few). Several glacial and interglacial cycles have influenced and shaped the morphology of these margins (Hjelstuen et al., 2007; Laberg et al., 2000; Laberg and Vorren, 2000; Vanneste et al., 2006). Apart from glaciation, other triggering mechanisms proposed for mass-wasting in the region include earthquakes, gas hydrate dissociation, high sedimentation rates, volcanism, and fluctuations in sea level conditions (Alves, 2015; Berndt et al., 2004; Bryn et al., 2005; Bünz et al., 2003;

Kvalstad et al., 2001; Haflidason et al., 2003; Laberg et al., 2000; Laberg and Vorren, 1995, 2000; Mienert et al., 2003).

Due to the different glacial events, the thick Cenozoic sedimentary successions in the Sørvestsnaget Basin have been, for several decades regarded as glaciogenic wedges. They are often linked to Neogene glaciation that affected the entire Barents Sea (Faleide et al., 1984; Ryseth et al., 2003; Sættem et al., 1994; Safronova et al., 2014). Notwithstanding the great contributions from these authors, a major constraint to their works is the general lack of stratigraphic control and high-quality data to observe the detailed composition of these sediments. For this reason, earlier workers in the Sørvestsnaget Basin and surrounding basins have focused on defining the boundaries of these wedges or understanding the evolution and architecture of the older sediments of the Eocene and Cretaceous ages (Faleide et al., 1984; Myhre et al., 1982; Safronova et al., 2014).

Based on the information above, the aims of this work are thus: a) to understand the types of mass-wasting deposits in the Sørvestsnaget Basin ; b) to evaluate the trigger mechanism and mode of propagation of mass-wasting deposits; and c) to assess the influence of glacial and non-glacial erosion as a control on slope instability in the study area. The paper starts with a brief description of the regional geology of the Barents Sea and the Sørvestsnaget Basin, moving on to discuss how the shelf-edge trajectory unravels the history of basin fill and sea level conditions. The discussion highlights the importance of mass wasting in the study area, the type of the deposits interpreted, and their possible mode of propagation. Mass-transport deposits (MTDs) in this work include any sedimentary package formed after one or multiple mass-wasting events. Clinoform describes a complete set of sigmoidal-shaped surfaces characterized by a topset, foreset and bottomset (see Johannessen and Steel, 2005: Patruno et al., 2015; Steel and Olsen, 2002). The topset of the shelf-margin clinoforms is the morphological shelf; the upper rollover of the clinoforms is the "shelf-slope break", and "slope" is the deeper-water surface below (Johannessen and Steel, 2005; Safronova et al., 2014).

2. Geological Setting

The Sørvestsnaget Basin is located in the Barents Sea (Figure 1a). The Barents Sea is an epicontinental sea that is characterised by several sedimentary basins, highs, and platforms, developed in response to complex tectonic processes (Faleide et al., 1984; Gernigon et al., 2014). The tectonic history of the entire Barents Sea begins with the Caledonian orogeny at ~400 Ma, followed by collision between Laurasia and Western Siberia at ~240 Ma. Extensional tectonic movements predominate during the Paleozoic to Paleogene development in the entire Barents Sea (Faleide et al., 1993; Johansen et al., 1999; Gudlaugsson et al., 1998; Worsley, 2008). The Cenozoic development of the Barents Sea was related to the opening of the Norwegian and Greenland Seas and the formation of a sheared margin in the west (Faleide et al., 2008). Seafloor spreading between Norway and Greenland began in the Early Cenozoic times (Eldholm and Thiede, 1980; Mosar et al., 2002). Early Cenozoic deformation includes wrench movement along the SW-NE trend faults and the progressive formation of pull-apart basins in the westernmost parts of the Barents Sea (Fiedler and Faleide, 1996; Gernigon et al., 2014).

Continental sedimentation in the Barents Sea is locally restricted to orogenic collapse basins during the Late Paleozoic to Early Mesozoic times (Faleide et al., 2008). Marine sedimentation was prevalent from the Late Paleozoic until recent times (Dalland et al., 1988a; Worsley, 2008). The Silurian to Early Devonian period witnessed large-scale erosion and exhumation of

Caledonian highs (Smelror et al., 2009). During the Devonian to Early Carboniferous times, exhumation and extensive erosion was dominant in hinterland areas (Gernigon et al., 2014). Carbonate deposition with evaporite intervals prevailed over wide areas of the Barents Sea shelf in Carboniferous and Permian times. This is in response to changes in tectonic setting and climatic conditions when the Barents Sea area drifted northwards from a paleo latitude of 20˚N in the Carboniferous to 55˚ (Doré 1995, Nilsen et al., 1995). Transgressive to regressive cycles of marine, deltaic and continental clastics were deposited in the Lower to Middle Triassic (Glørstad-Clark et al., 2010). Late Triassic to Early Cretaceous times are periods of post-rift thermal subsidence and renewed tilting of blocks (Faleide et al., 1993 and Worsley, 2008). In general, regional subsidence and the formation of a huge interior sag basin characterised the entire Barents Sea during the Mesozoic (Doré, 1995). Contrastingly, uplift and erosion was predominant in the entire SW Barents Sea during the Cenozoic (Dimakis et al., 1998; Faleide et al., 1996). As a result, Neogene glaciations in the northern hemisphere caused an intense deposition of thick sediments in the oceanic basins west of the Barents Sea (Faleide et al., 1996).

The Sørvestsnaget Basin (Figure 1) represents the SW structural continuation of the Bjørnøya Basin. A group of normal faults of Tertiary age separates both basins (Faleide et al., 1988; Gabrielsen et al., 1990). The Sørvestsnaget Basin to the north is marked by the lavas of the Vestbakken Volcanic Province and by the NE-SW trending fault complexes on the southern part of Stappen High (Figure 1a). On the southeastern side of the Sørvestsnaget Basin is the Senja Ridge and Veslemøy High, whereas it is marked by the oceanic crust to the west (Figure 1a). Stratigraphic successions in the Sørvestsnaget Basin includes thick sediments of Cretaceous and Tertiary age (Gabrielsen et al. 1990). The basin has experienced significant subsidence since the Early Cretaceous times, thus providing accommodation space for the deposition of very thick Cretaceous and Tertiary sediments (Ryseth et al, 2003). The presence of these thick Cretaceous to Tertiary sediments in the basin makes it hard to identify the pre-Cretaceous succession. The crystalline basement is about 17 km underneath most of the basin (Mjelde et al., 2002). In addition, the presence of salt diapirs in the southern part of the Sørvestsnaget Basin can indicate that the area probably developed as a sedimentary basin in the Late Palaeozoic times (Knutsen and Larsen, 1997). Cretaceous to Tertiary successions in the basin include deep marine sediments of the Sotbakken Group, and younger marine to glacial sediments of the Nordland Group (Dalland et al., 1988). The intra-Miocene to Oligocene unconformity separates the Nordland Group from the Sotbakken Group (Dalland et al., 1988).

3. Data and Methods

The primary dataset for this study consists of 2D seismic reflection data, core photographs and wireline logs from two boreholes (Figure 1b). The 2D seismic data are a high quality, high-resolution dataset composed of 79 lines with a grid spacing of 4 x 4 km. The vertical sampling rates and the recording length for the data are 4 ms and 9,200 ms, respectively. Line orientation is NE-SW, perpendicular to the orientation of the basin, and NW-SE (Figure 1b). The seismic lines are in the time domain and are zero-phase at the seabed. The processing algorithm for the seismic data includes demultiplexing and pre-stack time migration using the 3D-Geo Kirchhoff algorithm. With a dominant frequency of 50 Hz and interval velocity of 2,200 m/s the vertical resolutions for the seismic data is ~11 m.

Two exploration wells were used in this study, 7216/11-1S and 7316/5-1 (Figure 1b). Borehole 7316/5-1 penetrated down to the Late Cretaceous interval at a measured depth of 4,027 (m). The second borehole intersected the Paleocene interval at a depth of 4,239 (m). Standard wireline logs used for the interpretation of lithology include gamma ray- GR, deep resistivity-RDEP, neutron-NEU, density-DEN and sonic- DT. Further interpretation of the lithology and sedimentary structures within the intersected intervals derives from photographs of conventional cores and samples. Cutting descriptions from the mud log provided additional information for interpretation of the lithology.

The main workflow used in this work is shown in Figure 2. The seismic interpretation included mapping of ten horizons, which are the boundaries of major depositional units, the tops and bases of seven mass-transport deposits, the base of thirteen channels and twelve v-shaped features/canyons. Fault interpretation provided an overview of the structural evolution of the margin. In addition to seismic and fault interpretation, clinoforms within the major depositional units were interpreted, and the variation in the position of the shelf-edge was analyzed and displayed on structural maps. The interpreted shelf-margin clinoforms are several 100s m high and more than 50 km in length. The shelf-edge trajectory is defined by the sequential migration of the shelf-slope break in a stratigraphic succession (Steel and Olsen, 2002), and it represents the evolution of the shelf edge during the development of a given group of clinoforms (Carvajal and Steel, 2006).

In the study area, the shelf-edge trajectory is categorized as a very low-angle ascending trajectory, a high angle ascending trajectory, a flat trajectory and a descending trajectory (Figure 2a). Ascending shelf-edge trajectories may result from ascending regressive shorelines with sands that have a higher potential to accumulate on the slope rather than on the basin floor (Johannessen and Steel, 2005). Ascending trajectories will result in a sigmoidal seismic pattern and long-term rise in relative sea level. Flat and descending trajectories will produce an oblique progradational seismic pattern. A flat trajectory suggests a stable, relative sea level through time, usually formed by optimal sediment supply. A descending trajectory may signify a large sediment supply influenced by a strong fluvial input (Johannessen and Steel, 2005). The shelf edge and slope morphology are characterized by channelized sediment transport conduits, such as canyon and gullies, which are favorable for sand delivery to the basin floor (Helland-Hansen and Hampson, 2009; Steel and Olsen, 2002).

Mass-transport deposits (MTDs) have distinctive tops and basal shear surfaces. Internally, the MTDs are transparent to chaotic seismic reflections (Figure 2b). Their tops are ridged and irregular, while their bases are delimited by a well-defined basal shear surface (Bull et al., 2009; Omosanya and Alves, 2013a; Posamentier and Kolla, 2003; Richardson et al., 2011). The basal shear surface separates disrupted strata within the MTD from the much more continuous deposits underneath (Frey Martinez et al., 2005). The upslope section of most of the MTDs is an extended headwall region, while their downslope part consists of compressed or thrusted sediments. The channels and canyons are erosional features characterized by onlap seismic reflections on their margins and by contrasting amplitudes between their fill and adjacent overbank deposits (*cf.* Gamboa et al., 2012; Posamentier and Kolla, 2003). To convert the seismic units to their equivalent well tops, the depth conversion formula was taken from a graph of depth (m) to travel-time (ms), using check shots data from the two interpreted boreholes (Figure 2c).

4. Results

4.1 Interpreted horizons and sedimentary packages

Ten horizons inferred as the boundary of major depositional units or Formations define the five principal sedimentary packages discussed in this work (Figure 3). The oldest units correspond to the top Kviting Formation, which is Paleocene in age, whereas the youngest horizon is the seabed. All the interpreted horizons belong to both the Torsk and the Kviting Formation (Figure 4a).

Package 1 (Paleocene to Oligocene)

The lower boundary of package 1 (P1) is the Paleocene horizon, while it's top is a reflector of Oligocene age (Figure 3). Both horizons are high-amplitude, continuous and relatively faulted. Package 1 is the bottom-most package and it defines the upper tips of most of the interpreted faults. In the southern part of the study area, package 1 thins toward the Sørvestsnaget Marginal High (Figure 3), with the latter High being a fault-bounded salt anticline. Package 1 generally thins towards the southwest and thickens in the northeastern direction. At the uppermost section of Package 1, there are several high-angle ascending clinoforms of Eocene age (Figure 3). Unlike the younger packages (P2 to P5), package 1 is devoid of mass-transport deposits and sub-marine channels.

In terms of lithology type and sedimentary structures, package 1 consists of interbedded shale, sandstone, and carbonate stringers (Figure 4b). The sandstones at the bottom of the interval have a low gamma ray response and highly contrast with the shale above and below it. The core photograph from borehole 7216/11-1S revealed a fine-grained sandstone that is approximately 2 m thick with some pebbly and angular rock fragments at a depth of 2988-2989 MD (Figure 5a and 5b). The sandstone have a dipping contact with the shale interval below (Figure 5c). In addition, the sandstone at the upper part of P1 also has a lower gamma ray value and the core data at this depth revealed a series of very fine to medium-grained sandstone with several sedimentary structures such as parallel lamination, ripple cross-lamination, bioturbations, flame structures, mud couplets, mudstone clasts and planar cross stratification (Figures 5f and 5g).

Debris flow deposits found at different intervals within the core are suggestive of a deep marine environment.

Package 2 (Miocene to Early Pliocene)

The diagnostic characteristics of package 2 (P2) are several V-shaped features interpreted within it. The upper part of P2 is of Lower Pliocene age, while the entire package is Miocene in age (Figure 3). Package 2 includes several high-amplitude and continuous reflectors. Similarly, package 2 thickens to the northeastern part of the study area. The clinoforms in this interval are up to 950 m high and more than 40 km long on the average (Figure 3). At the top of package 2, clinoforms, with respect to the position of the inferred shelf-edge, show a generally flat to descending trajectory. Several negative high-amplitude anomalies (HAA) or fluid-flow features are common in the northeastern part of the study area (Figure 3). Package 2 consists of interbedded sandstone and shale, with some volcanic sediment described as tuff from cuttings in borehole 7216/11-1 (Figure 4b). The core photograph from borehole 7316/5-1 shows that Package 2 consists of massive, coarse to very coarse-grained sandstone with some angular to rounded rock fragments, an indication of debris flow deposits (Figures 5d and 5e).

Packages 3 to 5 (Mid Pliocene to Recent)

Package 3 (P3) is delimited by mid-Pliocene reflectors and clinoforms with descending trajectories (Figure 3). The base of package 3 erodes the upper part of some of the V-shaped features within package 2. The thickness of P3 increases towards the southwest, thus contrasting the pattern observed in P2 and P1. In addition, the reflectors become more discontinuous, transparent and with a lower amplitude relative to the older packages (Figure 3).

Package 4 (P4) consists of discontinuous, low amplitude and transparent reflectors. Package 4 thins to the northeast and thickens in the southwest direction like package 3 (Figure 3). Clinoforms within the package have a high-angle ascending trajectory. The youngest package in the study area is package 5 (P5), which is composed of low-angle ascending clinoforms. Several high-amplitude anomalies are located within this package. In addition, package 5 thickens towards the SW and forms the upper part of the Nordland Group. Package 5 is Pleistocene in age (Ryseth et al., 2003; Safranova, 2014).

Packages 3 and 4 have high gamma values with frequent incursions of low-gamma sediments, which consist of shale, with several sandstone intercalations (Figure 4b). Package 5 shows low radioactivity content in 7316/5-1 and a higher gamma reading in 7216/11-1S, thereby implying that the package is sandier in the northern part of the study area.

4.2 Interpreted Mass-transport deposits

The seven MTDs interpreted in the study area range in age from Miocene (MTD1) to Pleistocene (MTD 6 and 7). All the MTDs have their inferred headwall region in the NE part of the seismic data (Figure 6). MTD 1 is approximately 1078 km^2 in area, and it comprises of chaotic, transparent and homogeneous packages on seismic sections (Figures 6 and 7a, Table 1). The toe region of MTD 1 comprises of subtle imbricate structures, while its upslope section is thinner as compared to the rest of the MTD. A ramp separates the thin region from the thicker downslope section by (Figure 7a).

In contrast to MTD 1, mass-transport deposits 2 and 3 comprise heterogeneous mixtures of moderately to highly deformed and highly faulted units on seismic sections (Figures 7a). A promontory separates MTD 2 from MTD 3 and MTD 4 in map view and on the seismic section (Figures 6b and 7a). The headwall region of MTD 2 is in the northern part of the study area (Figure 6b and 6c). MTD 2 measures approximately 1,343 km^2 in area, with approximately 872 km3 of sediments possibly translated during this event (Table 1). MTD 2 shows a N-S direction of transport (Figure 6b and 6c).

The internal configuration of MTD 3 includes a high-amplitude and faulted sequence in the transition zone, with low to moderate amplitude at its upslope and downslope sections, respectively (Figure 7b). Extensional features dominate the headwall region, while the toe region is not on the current seismic data (Figure 7b). In terms of area coverage, MTD 3 is about 360 km2 in area, with 119 km^3 of sediments remobilized (Table 1). The headwall region of MTD 4 is ENE of the Sørvestsnaget Basin, comprising about 281 km^3 of sediment remobilized from the ENE to the WSW part of the seismic data (Figure 6c and Table 1). The seismic character of MTD 4 includes slump and debrites facies (Figure 7a).

The largest MTD in this study is MTD 5, which is 12,185 km^2 in area, and has a volume of 3,351 km^3 (Table 1, Figures 7a and 7b). MTD 5 is oriented NE-SW (Figure 6a). On seismic sections, the MTD is composed entirely of chaotic debrites in the NW part of the seismic to heterogeneous mixture of low-amplitude and high-amplitude disrupted masses at the position of the shelf-break (Figures 7a and 7b). The lithological composition of MTD 5 as revealed from borehole 7216/11-1S includes vertical succession of sandy shale interlayered with thin mudrock (Figure 8). The gamma ray value is intermediate, with about 40 to 50 API in the sandy shale and reaching up to 100 API in the mudrock. Sonic transit time is high (up to about 160 us/ft) and resistivity is intermediate about 10 ohm.m, while interval velocity is less than 2000 m/s (Figure 8). Other characteristics of MTD 5 include the presence of rafted blocks and an internal detachment surface within the MTD (Figures 7a, 9a and 9b). The rafted blocks are common from the shelf-edge position into the slope (Figure 7a). Additionally, MTD 5 is composed of large-scale grooves at its base and negative high-amplitude or enhanced reflections beneath the basal shear surface (Figures 9a and 9c). The enhanced reflections are suggestive of gas accumulation in the subsurface (cf. Hovland and Judd, 1988).

MTDs 6 and 7 have a similar orientation as MTD 5 and an area coverage of about 2204 and 601 km^2, respectively (Figure 6a, 6d and Table 1). At the southern part of the study area, MTD 6 is characterized by a vertical succession of high-amplitude continuous reflectors (hemipelagic), interlayered by a chaotic mass of debrites (Figure 10). The hemipelagic sediments are common at the upper slope section of the study area and are apparently remobilized sediments. The dominant seismic facies within MTD 6 and 7 are debrites (Figure 7a and 10). MTD 7 shows a distinct crosscutting relationship with MTD 5. This abrupt termination is the lateral margin of MTD 7 (Figure 10). In addition, the headwall region of MTD 7 is located close to the interfered shelf edge of package 5 (Figure 6a).

4.3 V-shaped canyons

Approximately twelve (12) v-shaped canyons (V1 to V12) are interpreted within sediment package 2 (Figures 3 and 11). The V-shaped features are located away from the Miocene shelf-break and are orientated dominantly in the NE-SW direction (Figure 11 and 12). The burial depth of the canyons is approximately 1375 to 1980 m subsea (Figures 3, 12a and 12b). In terms of shelf to slope morphology, the canyons are located about 11 km (V8) and up to 29 km (V1) from the position of the Miocene Shelf Break (Figure 11). At their lower slope position or away from the shelf, the canyons lack lobes and are generally abutted against the Sørvestsnaget Marginal High (Figure 11).

On seismic sections, the v-shaped canyons cut and incise the adjacent sediments (Figure 12). Their internal reflection configuration includes medium to low amplitude chaotic sediments that onlap seismic reflections on their margins (Figures 3, 12a and 12b). In some of the v-shaped canyons, the internal reflectors are continuous, parallel to sub-parallel reflectors (Figure 12a). The overlying package 3, termed as P3, eroded the upper parts of majority of the canyons (Figure 3). The canyons are characterized by a heterogeneous composition of high and low amplitude and are likely to be sand rich (e.g. V9 and V11). While those with low amplitude, parallel and continuous reflectors are likely mud-rich (e.g. V1). Borehole 7216/11-1S intersected the northwest margin of canyon V1 and on wireline logs; it is composed of mudrock with an interval velocity of about 2,000 km/s (Figure 13).

Geometrically, the canyons have a maximum length (L) of 39–66 km and maximum width (B) of 6 to 19 km (Figure 11 and Table 2). Area coverage of the canyons ranges from about 88 km^2 (V6) to approximately 248 km^2 (V3). At their deepest part, the height of the canyon can reach up to about 1 km (V5, V9). Height (D) of all canyons is defined by $0.87 < D < 0.97$ (Table 2). Aspect ratio (B/D) of the canyons is the ratio of breadth to depth. In the study area, the canyons have a maximum value of B/D of 17 and a minimum of 7. There is positive correlation between the breadth and length of the canyons (Figure 14a). The coefficient of correlation is up to 0.6. The average gradient within the canyons is about 1.480 towards their deepest part (Table 2). The plot of gradient against the height of the canyons show a negative correlation with coefficient of about 0.5 (Figure 14b).

4.4 Submarine Channels

The thirteen (13) submarine channels (Ch1 to Ch13) discussed in this work include isolated and vertically stacked types (Figure 11). Five of the interpreted channels are isolated, while the remainder are vertically stacked. All of the channels are located on the morphologic shelf of the Pliocene 3 reflector except Ch. 13, which is located on the slope. Hence, the channels are submarine channels (Figure 11). The length and breadth of the channels varies from 13 km to 83 km and 3 km to 18 km, respectively (Table 3). Submarine channels in the study area have low positive correlation between their breadth and length. Coefficient of correlation between channel breadth and length is approximately 0.2 (Figure 14a). The longest channel in the study area is Ch1, which measures approximately 83 km in length (Figure 11, Table 3). Height (D) of the channels is on the average about 820 m. The aspect ratio (B/D) ranges from 4 to 21, with an average gradient of the channel being about 1.520 (Table 3). The plot of channel gradient against height/depth show almost zero correlation with coefficient of correlation of about 0.04 (Figure 14b). All the channels are beneath MTD 5 and they exhibit diverse orientations such as NW-SE, NE-SW and NNE-SSW (Figure 15).

The principal seismic facies within the vertically stacked channels include slumps, high to low amplitude reflectors towards the upper part and basal lag along the channel axis (Figure 15a and 15b). The channels incised into the subsurface, eroding the upper tip of the majority of the underlying faults (Figure 15). On seismic sections, the isolated channels have low-amplitude reflectors along their axes and hemipelagic to low amplitude reflection on their margins (Figure 15a). Conversely, the vertically stacked channels show a succession of varied amplitude reflections, with each channel being characterized by a distinctive, high amplitude base (Figure 15b).

Examples of vertically stacked channels include Ch4 to Ch8 and Ch10 to Ch12. These types of channels are restricted to the northwestern and eastern part of the study area (Figure 11). The vertically stacked channels in the NW part of the study area are orientated mainly in the NNE-SSW direction, while the one in the eastern part has a varied orientation (Figure 15b). Contrastingly, the isolated channels are oriented in the NE-SW direction (Ch1 and Ch13), NW-SE (Ch2) and NNW-SSE (Ch3 and Ch9).

5. Discussion

5.1 *Recurrence and types of mass-transport deposits in the study area*

The occurrence of mass-transport deposits across chronostratigraphic levels in the study area shows that mass-wasting is an inherent and recurrent event in the study area. Mass-transport deposits in the Sørvestsnaget Basin range in age from the Miocene to the Late Pleistocene times. On seismic sections, the MTDs include entirely homogeneous packages comprised of debrites that justify their long distance of travel and degree of mass-disaggregation, as compared to their heterogeneous counterparts (cf. Omosanya and Alves 2013a, Posamentier and Kolla, 2003). Heterogeneous MTDs have a sense of their original stratification preserved and are composed of sandy material. They have a shorter travel distance and a moderate to no internal deformation (Omosanya and Alves, 2013b). In the study area, MTDs 1 and 2 are examples of homogeneous MTDs, while MTDs 3 to 7 are heterogeneous deposits. Based on their chaotic appearance and composition of debrites seismic facies on seismic section, MTDs 1 and 2 are examples of debris flow deposits while MTDs 3 and 4 are slumps. The latter deposits are composed of a mixture of different MTD facies, that is, slide, debrites, slightly deformed strata, and any form beyond seismic resolution (cf. Gamboa et al., 2010; Omosanya and Alves, 2013a).

In the Sørvestsnaget Basin, MTD 5 to MTD 7 have a distinctive seismic facies character relative to the other heterogeneous deposits. Characteristically, their shelf position is dominated by debrites, slumps are a common feature of their shelf-break position and at their distal or part (i.e. slope) they are characterized by vertical succession of hemipelagites and debrites (Figures 7a and 7b). Therefore, MTD 5 to MTD 7 are classified as examples of large submarine fans or trough mouth fans situated in front of bathymetric troughs that extend across continental shelves to the shelf break and into the slope (Figures 6a, 6d and 11). Trough mouth fans consist of glaciogenic materials transported to the continental slope via debris flow processes (Cofaigh et al., 2003). The hemipelagic materials are interglacial or interstadial sediments and the number of debrites or debris flow deposits often signify the change in position of the shelf-edge (Laberg and Vorren, 1995; Vorren and Laberg, 1997). MTD 6 and MTD 7 show an obvious emergence from a bathymetric trough, as they are located in the proximity of the Pliocene 3 shelf edge (Figure 11). In addition, MTD 7 also extends from the position of the morphological shelf and into the slope. Based on these seismic and morphological characteristics, MTD 5 to MTD 7 are examples of trough mouth fans, TMFs (*cf*. Cofaigh et al., 2003; Vorren and Laberg, 1997).

5.2 *Trigger mechanism for mass-wasting and mode of propagation of the MTDs.*

We propose that the likely mechanisms driving mass-wasting or slope failure in the study area include an increased pore pressure from the sea-level fall and high sedimentation rate, glaciation, over-steepened slope, volcanism and gas hydrate dissociation. Fluctuations sea-level could have triggered MTD 1 to MTD 4, while MTD 5 to MTD 7 are products of Neogene glaciation. The next section discusses sea level fluctuations in the study area. High sedimentation may occur during sea level fall when the maximum sediments are at the shelf-slope break. As for gas hydrate dissociation, the study area is located in a zone suitable for gas hydrate formation (Chand et al., 2008; Laberg and Andreassen, 1996). Gas hydrate dissociation is the trigger mechanism for some of the most renowned and largest submarine landslides in the northeastern Atlantic margin (Brown et al., 2006; Bünz et al., 2003; Jansen et al., 1987; Lindberg et al., 2004; Mienert et al., 2005). The presence of several fluid anomalies at the base of most of the MTDs support evidence for gas and fluid being a trigger for slope failure in the basin (Figures 3, 9c and 9d).

As for glaciation and volcanism, the first evidence for glaciation in the Barents Sea is from the Fram Strait at about 15 Ma (Knies and Gaina, 2008; Solheim et al., 1998). Glaciation affecting the Barents Sea includes small-scale (14–15 Ma), medium-scale (2.7–8 Ma) and large-scale glaciation from 2.7 Ma to recent times. The melting of ice sheets can generate large-scale slope instability and produce mass-transport deposits (e.g. MTDs 5, 6 and 7 in this work). Furthermore, high slope gradients are important for the deposition the MTDs from the shelf into the basin. This is evident for the older MTDs 1 to 4 that are located farther from their shelf-edge position (Figures 6 and 11). MTD 1 is approximately 18 km, MTD is about 21 km, MTD 3 is almost 19 km and MTD 4 is on average 13 km from the Miocene Shelf Break (Figure 11). On the other hand, gentle or slope gradients of <10 are favorable for the development of MTDs 5 to 7 (TMFs) in this study (*cf*. Cofaigh et al., 2003). Evidence for multiple volcanic episodes is recorded on the northern part of the study in areas of the Vestbakken Volcanic Province (Faleide et al., 1988; Richardsen et al., 1991). These volcanic activities are related to opening of the Norwegian and Greenland Sea and the subsequent re-configuration in plate motion during the evolution of the Stappen High and the northern section of the Sørvestsnaget Basin (Faleide et al., 1988; Lundin and Doré, 2002).

For most MTDs, the removal of sediment from the headwall region will create a decrease in lithostatic stress in the orientation shown in Figure 16a. Consequently, the downslope translation and thickening of the remobilized sediments causes an overloading of the toe region. The transfer of load downslope will ignite a pressure gradient from the area under the MTD to the headwall region (Dykstra, 2005), which will encourage fluid flow along the bedding in an up-dip direction and increase the likelihood of failures. Three kinds of failures are possible under this scenario (Figures 15b–15d): Progressive failures, where a series of failures sequentially cut further downdip (Figure 16b). In this situation, the movement of remobilized sediments is entirely at downslope locations of the original headwall scarp (Minisini et al., 2007; Schnellmann et al., 2005). Retrogressive failures happen when an initial failure surface exposes an unstable headwall that sequentially fails upslope until a stable headwall is achieved (Figure 16c). Whole-body failure involves initial movement throughout the entire failing mass at the same time, after which the mass may become internally deformed (Figure 16d).

Consequently, the MTDs in the study area show evidence for all the three mechanisms discussed above. Although progressive failure is poorly documented for most mass failures (Dykstra, 2005), MTDs 1 and 3 in the study area are thought to have formed through progressive failures. The presence of several extensional failures dipping towards the toe region within the two MTDs provides evidence for the increasing and sequential failure downslope. These extensional faults are essentially oriented parallel, and are located farther away from the headwall region (Figure 8). Retrogressive failures are a likely mechanism for MTDs 2 and 4. The headwalls of these two MTDs have small thicknesses due to the generation, during failure, of accommodation space on the seafloor (Dykstra, 2005; Lucente and Pini, 2003; Sawyer et al., 2009). MTDs 5, 6 and 7 seemingly developed through whole-body failure. These MTDs are translated apparently and exclusively ahead of ice streams. Failure occurred within the sediment mass at the same time prior to subsequent internal deformation. Figure 16e shows a conceptual model for the formation of trough mouth fans, as suggested by Vorren and Laberg (1997).

5. 3 Sea-level conditions, environment of deposition and sediment source area in the basin from Miocene to Pleistocene time.

The position of the shelf-edge was marked across each of the packages and the shelf-edge trajectory is shown in Figures 6 and 10. An important aspect to the shelf-edge trajectory is that it allows visualization of the traditional systems tracts as part of a more continuous spectrum of deposition during relative rise and fall of the sea level (cf. Helland-Hansen and Gjelberg, 1994). The shelf-edge position is a measure of the lateral and vertical shift of the slope-break and an indication of the area of significant change in depositional processes (Helland-Hansen and Hampson, 2009). In the study area, the shelf-edge shows a general NNW to SSE orientation, which occurred during the Miocene to late Pliocene times. The shelf-break trajectory revealed a westwards migration from the Miocene until the late Pliocene times (Figures 6 and 11). In the Early Paleocene times, the shelf-edge at the NNW margin of the study area showed a shift of about 5 km toward to the east. The southern part of the study area revealed the widest separation in the position of the shelf edge from the Miocene until recent times. Hence, the Sørvestsnaget Basin has witnessed fluctuating sea-level conditions associated with several cycles of progradation since the Miocene time until recent times.

In terms of the environment of deposition in the Sørvestsnaget Basin since the Eocene times, biostratigraphic data from sediment package 1 (P1) revealed the presence of radiolaria and agglutinated foraminifera and the absence of calcareous fossils (Norsk Hydro, 1993; Ryseth et al., 2003). Radiolaria are organisms with a skeleton composed of silica, while the agglutinated foraminifera have a test/shell composed of foreign particles (Boersma, 1998; Kling, 1998). The abundance of these two organisms combined with the absence of calcareous fossils indicates that the palaeo-environment was below the carbonate compensation depth (CCD), which is most likely a deep-water environment. The shelf-edge trajectory further favoured the latter assertion. The interpreted shelf-edge trajectory changed from high-angle ascending clinoforms in P1 (Eocene times), suggestive of sea level rise, landward backstepping of the shoreline and deposition of the deep marine succession. Flat to descending clinoforms in P2 and P3 (Miocene to Mid Pliocene) indicate a period of relative sea level fall and large sediment supply to the basin, leading into ascending clinoforms in P4 and P5 (Late Pliocene to Pleistocene). The trajectory of the clinoforms within P4 and P5 imply sea-level rise and lower sediment supply (Helland-Hansen and Hampson, 2009; Steel and Olsen, 2002). Hence, the environment of deposition in the study area was deep-water in the Eocene to shallow marine in the Miocene and Pliocene, followed by deep-water in the late Pliocene to Pleistocene.

Figure 17 shows a conceptual model for the sediment source area to the Sørvestsnaget Basin. The figure shows that sediment supply to the basin was from the northeast in areas of the present-day Stappen High. On seismic sections, the shelf-margin clinoforms have a general southwest orientation, signifying sediment supply from the northeastern area (Figure 3 and 16). However, the Stappen High evolved in the Late Paleozoic Era as a positive element. It subsided and later uplifted during the Early Cretaceous and Tertiary times in response to activity along the Knølegga Fault and Hornsund Fault complex and during the opening of the Norwegian-Greenland Sea in the Early Eocene period (Gabrielsen et al., 1990). The southern slope of Stappen High was formed by the inversion of the northwestern part of the Bjørnøya Basin during Early Cenozoic (Gabrielsen et al., 1997). Hence, sediments or clastic wedges in the Sørvestsnaget Basin are from Stappen High since the Eocene times.

5.4 Are MTDs in the study area products of glacial erosion?

In this work, we theorize that the mechanisms driving sediment transport in the study area are submarine erosion and glaciation. The presence of the v-shaped canyons and submarine channels is evidence for active subaqueous erosion during Miocene to Mid-Pliocene times. The channels and canyon incised the substrate and acted as conduits for sediment transport to the slope. Additionally, the flat to descending geometry of the clinoforms also favors possible transport of sediments or sands through canyons and gullies during this time (*cf.* Helland-Hansen and Hampson, 2009; Steel and Olsen, 2002). Collapse of canyon and channel walls could be one way of generating slope instability and slumps localized within the canyon and channel axis (*cf.* Deptuck et al., 2003).

In the Sørvestsnaget Basin, submarine canyons are predominant within the Miocene interval, where MTD 1 to 4 are interpreted. The prevalence of canyons during this time provided evidence for the likelihood of subaqueous non-glacial erosion. We suggest slope instability during the Miocene was influenced by high sediment supply to the slope and sediments transport the canyons rather than glaciation. Consequently, by comparing the size and volume of the different MTDs, from Table 1 and Figure 6, it is evident that the younger MTDs 5, 6 and 7 are larger as compared to the earliest MTDs 1 to 4, and could only have been connected to glaciation. Since the first glacial events are small-scale as compared to larger-scale glaciation of late Pliocene times, we can therefore hypothesize that the larger volume of sediments remobilised by MTDs 5, 6 and 7 are the products of large-scale glaciations (Figures 6, 7a and 7b). Further evidence for the dominance of non-glacial erosion during the translation of MTD 1 to 4 in the Miocene to Mid Pliocene times includes a) the restriction of all the submarine channels to the base of MTD 5 and b) sea-level fall or descending geometry of the clinoforms from Miocene to Early Pliocene times. The maximum fall in sea level occurred during the Early Pliocene with sediment supply to the shelf edge presumably at its maximum during this time (Figure 17; c*f*. Masson et al., 1997; Posamentier and Kolla, 2003).

In this study, the formation of the v-shaped canyons remains poorly understood. Jobe et al. (2011) recognized two main types of submarine canyons along the continental margin of Equatorial Guinea. ‘Type I’ canyons indent the shelf edge and connected to areas of high sediment supply, generating erosive canyon morphologies, sand-rich fill and large downslope submarine fans/aprons. These types of canyon are composed of erosive, sandy turbidity currents and mass-wasting (Jobe et al., 2011). The type II canyons do not indent the shelf edge and they exhibit smooth to highly aggradational morphologies. Type II canyons have mud-rich fill with no downslope fans/aprons.

The v-shaped canyons in this work bear similarity to the type I canyon of Jobe et al. (2011), in terms of their geometry, association with mass-wasting and the presence of sands within their axis. However, canyons in this work lack downslope aprons or lobes, unlike the Type I of Jobe et al., (2011). In addition, they do not show any direct indentation of the shelf edge. The lack of downslope aprons or fans may be due to tectonic influence, or the presence of a barrier. The Sørvestsnaget Marginal High is likely a structural barrier to the deposition of these aprons, thereby reducing the slope gradient and energy of the flow. Hence, the canyons are single-stage canyons formed over a relatively short period. The likelihood of mud-rich or type II canyon is also suggested by the petrophysical data from borehole 7216/11-1S and the parallel to continuous reflectors common within some of the canyons (Figures 12 and 13). Hence, canyons in the study area do not fit perfectly into any of the descriptions suggested by Jobe et al. (2011).

6. Conclusions

1. The Sørvestsnaget Basin developed in response to multiple processes from the Miocene to recent times. These processes include the retrogradation and backstepping of the shoreline, progradation and slumping, or mass-wasting. The shelf-margin trajectory essentially shows a westward migration since Miocene times, with sea-level fluctuations recorded by alternating cycles of ascending, flat and descending shelf margin clinoforms.
2. Mass-wasting is a recurrent process in the Sørvestsnaget Basin, SW Barents Sea. The seven mass-transport deposits (MTDs) interpreted in this work range in age from the Late Miocene to Holocene times. These MTDs include homogeneous and heterogeneous units on seismic sections.
3. Triggering mechanisms for slope failure in the basin may include increased pore pressure from sea-level fall and high sedimentation rate, over-steepened slope, glaciation, volcanism and gas hydrate dissociation. The study area is located in a zone suitable for gas hydrate formation. Evidence for multiple volcanic activities is recorded on the northern part of the study in areas of the Vestbakken Volcanic Province.
4. The oldest MTDs show a closer link to the submarine canyons, while the younger MTDs are the products of large-scale Neogene glaciation that affected the entire Barents Sea margin. Evidence for subaqueous erosion includes several v-shaped canyons and submarine channels buried beneath MTD 5. The v-shaped canyons extend farther from the shelf-edge position and abut against the Sørvestsnaget Marginal High.

5. Mass-wasting in the study area occurred through progressive, retrogressive and whole body or coherent downslope failures.

Acknowledgement

We appreciate the technical and financial support of Multi Client Geophysical (MCG) towards the successful completion of this research. We express our gratitude to them for the permission to publish this work. Further appreciation to the Norwegian Petroleum Directorate (NPD) for access to the borehole data used in this research and Schlumberger for provision of Petrel® for seismic interpretation. This work is also sponsored by the ARCEx project (Research Centre for Arctic Petroleum Exploration) which is funded by the Research Council of Norway (grant number 228107) together with 10 academic and 9 industry partners.

References

Alves, T.M., 2015. Submarine slide blocks and associated soft-sediment deformation in deep-water basins: A review. Mar. Pet. Geol. 67, 262–285. doi:10.1016/j.marpetgeo.2015.05.010

Berndt, C., Bünz, S., Clayton, T., Mienert, J., Saunders, M., 2004. Seismic character of bottom simulating reflectors: examples from the mid-Norwegian margin. Mar. Pet. Geol. 21, 723–733. doi:10.1016/j.marpetgeo.2004.02.003.

Boersma, A., 1998. 2 - Foraminifera, in: Haq, B.U., Boersma, A. (Eds.), Introduction to Marine Micropaleontology (Second Edition). Elsevier Science B.V., Amsterdam, pp. 19–77.

Brown, H.E., Holbrook, W.S., Hornbach, M.J., Nealon, J., 2006. Slide structure and role of gas hydrate at the northern boundary of the Storegga Slide, offshore Norway. Mar. Geol. 229, 179–186. doi:10.1016/j.margeo.2006.03.011

Bryn, P., Berg, K., Forsberg, C.., Solheim, A., Kvalstad, T.., 2005. Explaining the Storegga Slide. Mar. Pet. Geol. 22, 11–19.

Bull, S., Cartwright, J., Huuse, M., 2009. A review of kinematic indicators from mass-transport complexes using 3D seismic data. Mar. Pet. Geol. 26, 1132–1151. doi:10.1016/j.marpetgeo.2008.09.011

Bünz, S., Mienert, J., Berndt, C., 2003. Geological controls on the Storegga gas-hydrate system of the mid-Norwegian continental margin. Earth Planet. Sci. Lett. 209, 291–307. doi:10.1016/S0012-821X(03)00097-9

Carvajal, C.R., Steel, R.J., 2006. Thick turbidite successions from supply-dominated shelves during sea-level highstand. Geology 34, 665–668. doi:10.1130/G22505.1

Chand, S., Mienert, J., Andreassen, K., Knies, J., Plassen, L., Fotland, B., 2008. Gas hydrate stability zone modelling in areas of salt tectonics and pockmarks of the Barents Sea suggests an active hydrocarbon venting system. Mar. Pet. Geol. 25, 625–636. doi:10.1016/j.marpetgeo.2007.10.006

Cofaigh, C.Ó., Taylor, J., Dowdeswell, J.A., Pudsey, C.J., 2003. Palaeo-ice streams, trough mouth fans and high-latitude continental slope sedimentation. Boreas 32, 37–55. doi:10.1080/03009480310001858

Dalland, A., Worsley, D., Ofstad, K., 1988. A lithostratigraphic scheme for the Mesozoic and Cenozoic succession offshore mid- and northern Norway. NPD Bull. 4.

Deptuck, M.E., Steffens, G.S., Barton, M., Pirmez, C., 2003. Architecture and evolution of upper fan channel-belts on the Niger Delta slope and in the Arabian Sea. Mar. Pet. Geol. 20, 649–676.

Dimakis, P., Braathen, B.I., Faleide, J.I., Elverhøi, A., Gudlaugsson, S.T., 1998. Cenozoic erosion and the preglacial uplift of the Svalbard–Barents Sea region. Tectonophysics 300, 311–327. doi:10.1016/S0040-1951(98)00245-5

Doré, A., 1995. Barents Sea Geology, Petroleum Resources and Commercial Potential. Arctic 48, 207–221.

Dykstra, M., 2005. Dynamics of Sediment Mass-Transport from the Shelf to the Deep Sea. University of California, Santa Barbara,.

Eldholm, O., Thiede, J., 1980. Cenozoic continental separation between Europe and Greenland. Palaeogeogr. Palaeoclimatol. Palaeoecol. 30, 243–259. doi:10.1016/0031-0182(80)90060-7

Faleide, J.I., Gudlaugsson, S.T., Jacquart, G., 1984. Evolution of the western Barents Sea. Mar. Pet. Geol. 1, 123–150.

Faleide, J.I., Myhre, A.M., Eldholm, O., 1988. Early Tertiary volcanism at the western Barents Sea margin. Geol. Soc. Lond. Spec. Publ. 39, 135–146.

Faleide, J.I., Solheim, A., Fiedler, A., Hjelstuen, B.O., Andersen, E.S., Vanneste, K., 1996. Late Cenozoic evolution of the western Barents Sea-Svalbard continental margin. Impact Glaciat. Basin Evol. Data Models Nor. Margin Adjac. Areas 12, 53–74. doi:10.1016/0921-8181(95)00012-7

Faleide, J.I., Tsikalas, F., Breivik, A.J., Mjelde, R., Ritzmann, O., Engen, Ø., Wilsom, J., Eldholm, O., 2008. Structure and evolution of the continental margin off Norway and the Barents Sea. Episodes 31, 82–91.

Faleide, J.I., Vågnes, E., Gudlaugsson, S.T., 1993. Late Mesozoic-Cenozoic evolution of the south-western Barents Sea in a regional rift-shear tectonic setting. Mar. Pet. Geol. 10, 186–214. doi:10.1016/0264-8172(93)90104-Z

Fiedler, A., Faleide, J.I., 1996. Cenozoic sedimentation along the southwestern Barents Sea margin in relation to uplift and erosion of the shelf. Impact Glaciat. Basin Evol. Data Models Nor. Margin Adjac. Areas 12, 75–93. doi:10.1016/0921-8181(95)00013-5

Frey Martinez, J., Cartwright, J., Hall, B., 2005. 3D seismic interpretation of slump complexes: examples from the continental margin of Israel. Basin Res. 17, 83–108. doi:10.1111/j.1365-2117.2005.00255.x

Gabrielsen, R.H., Faerseth, R.., Jensen, L.N., Kalheim, J.., Riis, F., 1990. Structural elements of the Norwegian continental shelf. Part 1: The Barents Sea Region. NPD Bull. 33.

Gabrielsen, R.H., Grunnaleite, I., Rasmussen, E., 1997. Cretaceous and tertiary inversion in the Bjørnøyrenna Fault Complex, south-western Barents Sea. Mar. Pet. Geol. 14, 165–178. doi:10.1016/S0264-8172(96)00064-5

Gamboa, D., Alves, T., Cartwright, J., Terrinha, P., 2010. MTD distribution on a “passive” continental margin: The Espírito Santo Basin (SE Brazil) during the Palaeogene. Mar. Pet. Geol. 27, 1311–1324. doi:10.1016/j.marpetgeo.2010.05.008

Gamboa, D., Alves, T.M., Cartwright, J., 2012. A submarine channel confluence classification for topographically confined slopes. Mar. Pet. Geol. 35, 176–189. doi:10.1016/j.marpetgeo.2012.02.011

Gee, M.J.R., Gawthorpe, R.L., 2006. Submarine channels controlled by salt tectonics: Examples from 3D seismic data offshore Angola. Mar. Pet. Geol. 23, 443–458. doi:10.1016/j.marpetgeo.2006.01.002

Gernigon, L., Brönner, M., Roberts, D., Olesen, O., Nasuti, A., Yamasaki, T., 2014. Crustal and basin evolution of the southwestern Barents Sea: From Caledonian orogeny to continental breakup: Evolution of the Barents Sea. Tectonics 33, 347–373. doi:10.1002/2013TC003439

Gudlaugsson, S.T., Faleide, J.I., Johansen, S.E., Breivik, A.J., 1998. Late Palaeozoic structural development of the South-western Barents Sea. Mar. Pet. Geol. 15, 73–102. doi:10.1016/S0264-8172(97)00048-2

Haflidason, H., Sejrup, H.P., Berstad, I., Nygard, A., Richter, T., Lien, R., Berg, K., 2003. A weak layer feature on the northern Storegga slide escarpment in: In European Margin Sediment Dynamics Mienert J, Weaver P.P.E. Springer, Berlin, Germany, pp. 55–62

Helland-Hansen, W., Gjelberg, J.G., 1994. Conceptual basis and variability in sequence stratigraphy; a different perspective: Sedimentary Geology 92, 31–52.

Helland-Hansen, W., Hampson, G.J., 2009. Trajectory analysis: concepts and applications: Basin Research, v. 21/5, p. 454-483. Basin Res. 21, 454–483.

Hjelstuen, B.., Eldholm, O., Faleide, J.., 2007. Recurrent Pleistocene megafailures on the SW Barents Sea margin. Earth Planet. Sci. Lett. 258, 605–618.

Hovland, M., Judd, A.., 1988. Seabed Pockmarks and Seepages. Impact on Geology, Biology and the Marine Environment. Graham and Trotman Ltd, London.

Jansen, E., Befring, S., Bugge, T., Eidvin, T., Holtedahl, H., Sejrup, H.P., 1987. Large submarine slides on the Norwegian continental margin: Sediments, transport and timing. Mar. Geol. 78, 77–107. doi:10.1016/0025-3227(87)90069-7

Jobe, Z.R., Lowe, D.R., Uchytil, S.J., 2011. Two fundamentally different types of submarine canyons along the continental margin of Equatorial Guinea. Themat. Set Stratigr. Evol. DEEP-WATER Archit. 28, 843–860. doi:10.1016/j.marpetgeo.2010.07.012

Johannessen, E.., Steel, R.., 2005. Shelf-margin clinoforms and prediction of deepwater sands: Basin Research. Basin Res. 17, 521–550.

Kling, S.A., 1998. 9 - Radiolaria, in: Haq, B.U., Boersma, A. (Eds.), Introduction to Marine Micropaleontology (Second Edition). Elsevier Science B.V., Amsterdam, pp. 203–244.

Knies, J., Gaina, C., 2008. Middle Miocene ice sheet expansion in the Arctic: Views from the Barents Sea: ICE SHEET EXPANSION IN THE ARCTIC. Geochem. Geophys. Geosystems 9, n/a–n/a. doi:10.1029/2007GC001824

Knutsen, S.-M., Larsen, K.I., 1997. The late Mesozoic and Cenozoic evolution of the Sørvestsnaget Basin: A tectonostratigraphic mirror for regional events along the Southwestern Barents Sea margin? Mar. Pet. Geol. 14, 27–54. doi:10.1016/S0264-8172(96)00039-6

Kvalstad, T., Nadim, F., Harbitz, C., 2001. Deepwater geohazards; geotechnical concerns and solutions. Presented at the Offshore Technology Conference, Houston, Texas, pp. 207–217.

Laberg, J.S., Andreassen, K., 1996. Gas hydrate and free gas indications within the Cenozoic succession of the Bjørnøya Basin, western Barents Sea. Mar. Pet. Geol. 13, 921–940. doi:10.1016/S0264-8172(96)00038-4

Laberg, J.S., Vorren, T.O., 1995. Late Weichselian submarine debris flow deposits on the Bear Island Trough Mouth Fan. Mar. Geol. 127, 45–72. doi:10.1016/0025-3227(95)00055-4

Laberg, J.S., Vorren, T.O., Dowdeswell, J.A., Kenyon, N.H., Taylor, J., 2000. The Andøya Slide and the Andøya Canyon, north-eastern Norwegian–Greenland Sea. Mar. Geol. 162, 259–275.

Laberg, J.., Vorren, T.O., 2000. The Trænadjupet Slide, offshore Norway - morphology, evacuation and triggering mechanisms. Mar. Geol. 171, 95–114.

Lindberg, B., Laberg, J.S., Vorren, T.O., 2004. The Nyk Slide—morphology, progression, and age of a partly buried submarine slide offshore northern Norway. COSTA - Cont. Slope Stab. 213, 277–289. doi:10.1016/j.margeo.2004.10.010

Lucente, C.., Pini, G.., 2003. Anatomy and emplacement mechanism of a large submarine slide within a Miocene foredeep in the northern Apennines, Italy: a field perspective. Am. J. Sci. 303, 565–602.

Lundin, E., Doré, A.G., 2002. Mid-Cenozoic post-breakup deformation in the “passive” margins bordering the Norwegian–Greenland Sea. Mar. Pet. Geol. 19, 79–93. doi:10.1016/S0264-8172(01)00046-0

Masson, D., Van Niel, B., Weaver, P., 1997. Flow processes and sediment deformation in the Canary debris flow on the NW African continental rise. Sediment. Geol. 110, 163–179.

Masson, D., Watts, A., Gee, M.J.R., Urgeles, R., Mitchell, N., Le Bas, T.., Canals, M., 2002. Slope failures on the flanks of the western Canary Islands. Earth-Sci. Rev. 57, 1–35.

Mienert, J., Vanneste, M., Bünz, S., Andreassen, K., Haflidason, H., Sejrup, H.P., 2005. Ocean warming and gas hydrate stability on the mid-Norwegian margin at the Storegga Slide. Mar. Pet. Geol. 22, 233–244.

Mienert, J., Berndt, C., Laberg, J., Vorren, T.O., 2003. Slope instability of continental margins., in: Wefer, G., Billett, D., Hebbeln, D., Jørgensen, B., Schlüter, M., van Weering, T. (Eds.), Ocean Margin Systems. Springer Verlag, New York.

Minisini, D., Trincardi, F., 2009. Frequent failure of the continental slope: The Gela Basin (Sicily Channel). J. Geophys. Res. 114. doi:10.1029/2008JF001037

Minisini, D., Trincardi, F., Asioli, A., Canu, M., Foglini, F., 2007. Morphologic variability of exposed mass transport deposits on the eastern slope of Gela Basin (Sicily channel). Basin Res. 19, 217–240. doi:10.1111/j.1365-2117.2007.00324

Mjelde, R., Breivik, A.J., Elstad, H., Ryseth, A.E., Skilbrei, J.R., Opsal, J.G., Shimamura, H., Mu-rai, Y., Nishimura, Y., 2002. Geological development of the Sørvestsnaget Basin, SW Barents Sea, from ocean bottom seismic, surface seismic and potential field data. Nor. Geol. Tidskr. 82, 183–202.

Mosar, J., Lewis, G., Torsvik, T., 2002. North Atlantic sea-floor spreading rates: implications for the Tertiary development of inversion structures of the Norwegian–Greenland Sea. J. Geol. Soc. 159, 503–515.

Mulder, T., Cochonant, H.., 1996. Classification of offshore mass movements. J. Sediment. Res. 66, 43–57.

Myhre, A.M., Eldholm, O., Sundvor, E., 1982. The margin between Senja and Spitsbergen Fracture Zones: implications from plate tectonics. Tectonophysics 89, 33–50.

Omosanya, K.., Alves, T.M., 2013a. A 3-dimensional seismic method to assess the provenance of Mass-Transport Deposits (MTDs) on salt-rich continental slopes (Espírito Santo Basin, SE Brazil). Mar. Pet. Geol. 44, 223–239. doi:10.1016/j.marpetgeo.2013.02.006

Omosanya, K.., Alves, T.M., 2013b. Ramps and flats of Mass-Transport Deposits (MTDs) as markers of seafloor strain on the flanks of rising diapirs (Espírito Santo Basin, SE Brazil). Mar. Geol.

Patruno, S., Hampson, G.J., Jackson, C.A.-L., Dreyer, T., 2015. Clinoform geometry, geomorphology, facies character and stratigraphic architecture of a sand-rich subaqueous delta: Jurassic Sognefjord Formation, offshore Norway. Sedimentology 62, 350–388. doi:10.1111/sed.12153

Piper, D.J.., Cochonat, P., Morrison, M.., 1999. The sequence of events around the epicenter of the 1929 Grand Banks earthquake: initiation of debris flows and turbidity current inferred from sidescan sonar. Sedimentology 46, 79–97.

Posamentier, H.W., Kolla, 2003. Seismic geomorphology and stratigraphy of depositional elements in deep-water settings. J. Sediment. Res. 73, 367–388.

Richardsen, G., Henriksen, E., Vorren, T.O., 1991. Evolution of the Cenozoic sedimentary wedge during rifting and seafloor spreading west of the Stappen High, western Barents Sea. Cenozoic Geol. Nortwest Eur. Cont. Margin Adjac. Deep-Sea Areas 101, 11–30. doi:10.1016/0025-3227(91)90060-H

Richardson, S.E.., Richard, J.., Mark, B.., Grant, F.S., 2011. Structure and evolution of mass transport deposits in the South Caspian Basin, Azerbaijan. Basin Res. 23, 702–719.

Ryseth, A., Augustson, J.H., Charnock, M., Haugerud, O., Knutsen, S.-M., Midbøe, P.S., Opsal, J.G., Sundsbø, G., 2003. Cenozoic stratigraphy and evolution of the Sørvestsnaget Basin, southwestern Barents Sea. Nor. Geol. Tidsskr. 83, 107–130.

Sættem, J., Bugge, T., Fanavoll, S., Goll, R., Mørk, A., Mørk, M.B.., Smelror, M., Verdenius, J.., 1994. Cenozoic margin development and erosion of the Barents Sea: Core evidence from southwest of Bjørnøya. Mar. Geol. 118, 257–281. doi:10.1016/0025-3227(94)90087-6

Safronova, P.A., Henriksen, S., Andreassen, K., Laberg, J.S., Vorren, T.O., 2014. Evolution of shelf-margin clinoforms and deep-water fans during the middle Eocene in the Sørvestsnaget Basin, southwest Barents Sea. AAPG Bull. 98, 515–544. doi:10.1306/08221312208

Sawyer, D.E., Flemings, P.B., Dugan, B., Germaine, J.T., 2009. Retrogressive failures recorded in mass transport deposits in the Ursa Basin, Northern Gulf of Mexico. J. Geophys. Res. 114. doi:10.1029/2008JB006159

Schnellmann, M., Anselmetti, F.., Giardini, D., McKenzie, J.., 2005. Mass movement-induced fold-and-thrust belt structures in unconsolidated sediments in Lake Lucerne (Switzerland). Sedimentology 52, 271–289.

Solheim, A., Berg, K., Forsberg, C.., Bryn, P., 2005. The Storegga Slide complex: repetitive large scale sliding with similar cause and development. Mar. Pet. Geol. 22, 97–107. doi:10.1016/j.marpetgeo.2004.10.013

Solheim, A., Faleide, J.I., Andersen, E.S., Elverhøi, A., Forsberg, C.., Vanneste, M., Uenzelmann-Neben, G., Channell, J.E.., 1998. Late Cenozoic seismic stratigraphy and glacial geological development of the East Greenland and Svalbard-Barents Sea continental margins. Quat. Sci. Rev. 17, 155–184. doi:10.1016/S0277-3791(97)00068-1

Steel, R., Olsen, T., 2002. Clinoforms, Clinoform Trajectories and Deepwater Sands, in: Sequence Stratigraphic Models for Exploration and Production: Evolving Methodology, Emerging Models, and Application Histories: 22nd Annual. Society of Economic Paleontologists and Mineralogists, pp. 367–380.

Trincardi, F., Argnani, A., 1990. Gela submarine slide: a major basin wide event in the Plio–Quaternary foredeep of Sicily. Geo-Mar. Lett. 10, 13–21.

Urgeles, R., Locat, J., Dugan, B., 2007. Recursive failure of the Gulf of Mexico continental slope: Timing and causes, in: Submarine Mass Movements and Their Consequences, Edited by V. Lykousis, D. Sakellariou, and J. Locat. Springer, New York, pp. 209–219. doi:10.1007/978-1-4020-6512-5_22

Vanneste, M., Mienert, J., Bu¨ nz, S., 2006. The Hinlopen Slide: A giant, submarine slope failure on the northern Svalbard margin, Arctic Ocean. Earth Planet. Sci. Lett. 245, 373–388.

Varnes, D.., 1978. Slope movement types and processes., Schuster, R.L., Kruse, R.J. (Eds.), Landslides, Analysis and Control. : Special Report, 176. National Academy of Sciences, Washington.

Vorren, T.O., Laberg, J.S., 1997. Trough mouth fans — palaeoclimate and ice-sheet monitors. Quat. Sci. Rev. 16, 865–881. doi:10.1016/S0277-3791(97)00003-6

Worsley, D., 2008. The post-Caledonian development of Svalbard and the western Barents Sea. Polar Res. 27, 298–317. doi:10.1111/j.1751-8369.2008.00085.x

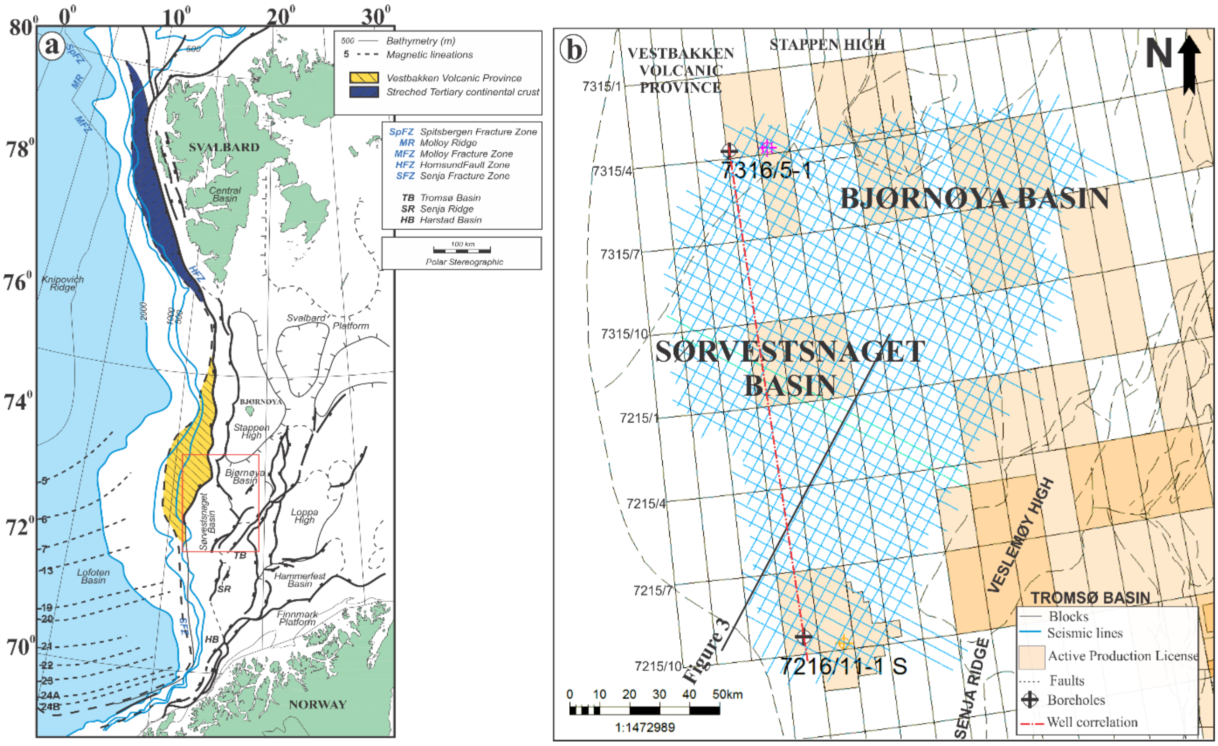

Figure 1: (a) Structural map of the SW Barents Sea Basins showing the location of the Sørvestsnaget Basin and the associated structural elements. The study area is a structural continuation of the Bjørnøya Basin. *The red box is the approximate location of the seismic survey*. (Modified after Ryseth et al., 2003); (b) Location of the seismic dataset used for this study. The data include multiple 2D seismic reflection lines acquired in 2011. Grid spacing for the data is 4 x 4 km with a vertical recording interval of 9.2 s. *The red dashed line is the correlation line between the two wells.*

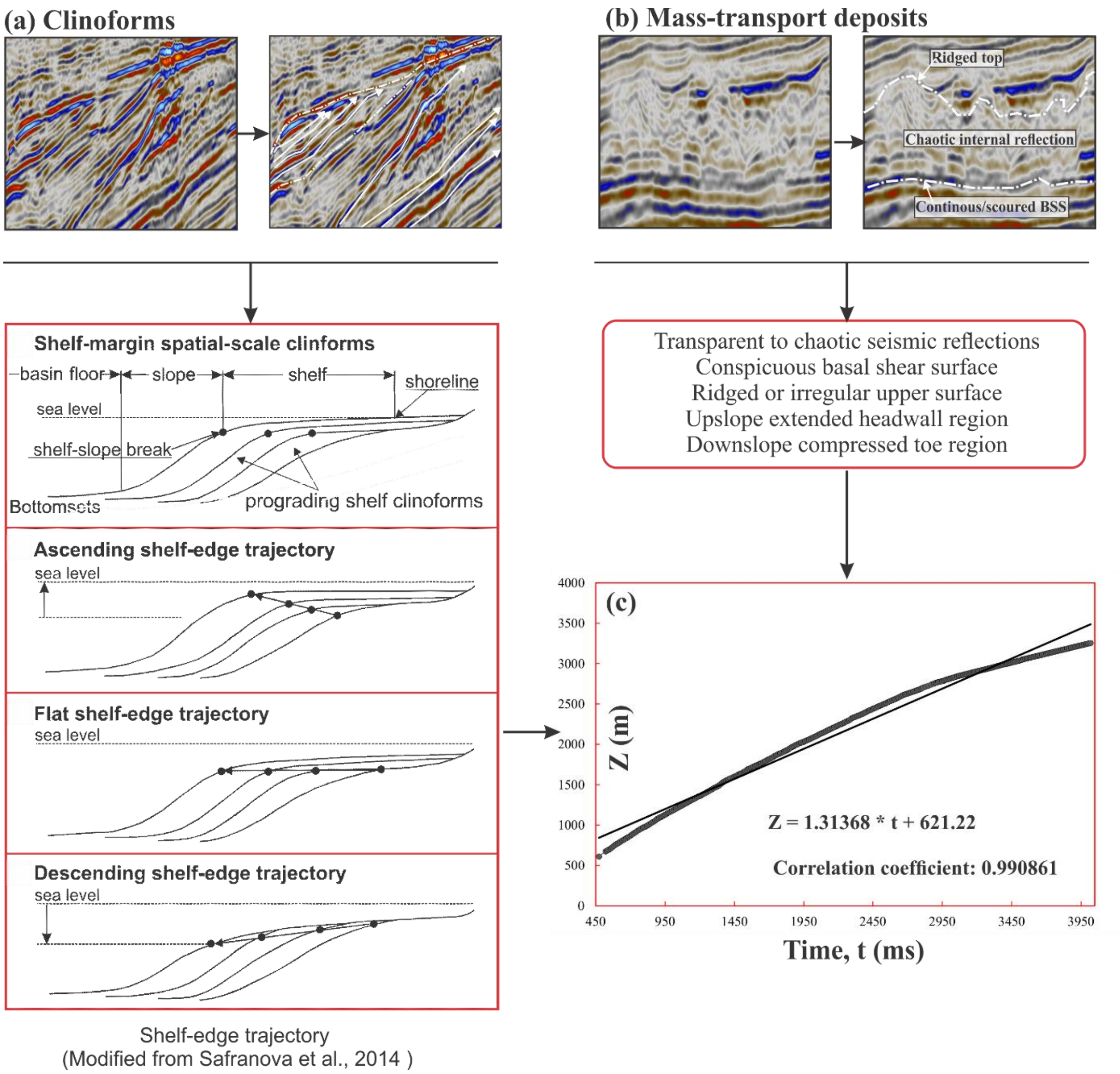

Figure 2: Research methodology and workflow used for this research includes (a) interpretation of shelf-margin clinoforms and their trajectory analysis. Structural maps display the positions of shelf-slope breaks in order to assess the evolution of the basin (b) the mass-transport deposits are transparent and chaotic packages on seismic sections and (c) depth (Z) to time (t) relationship used for depth conversion and calculation of the morphometric properties of the channels and canyons.

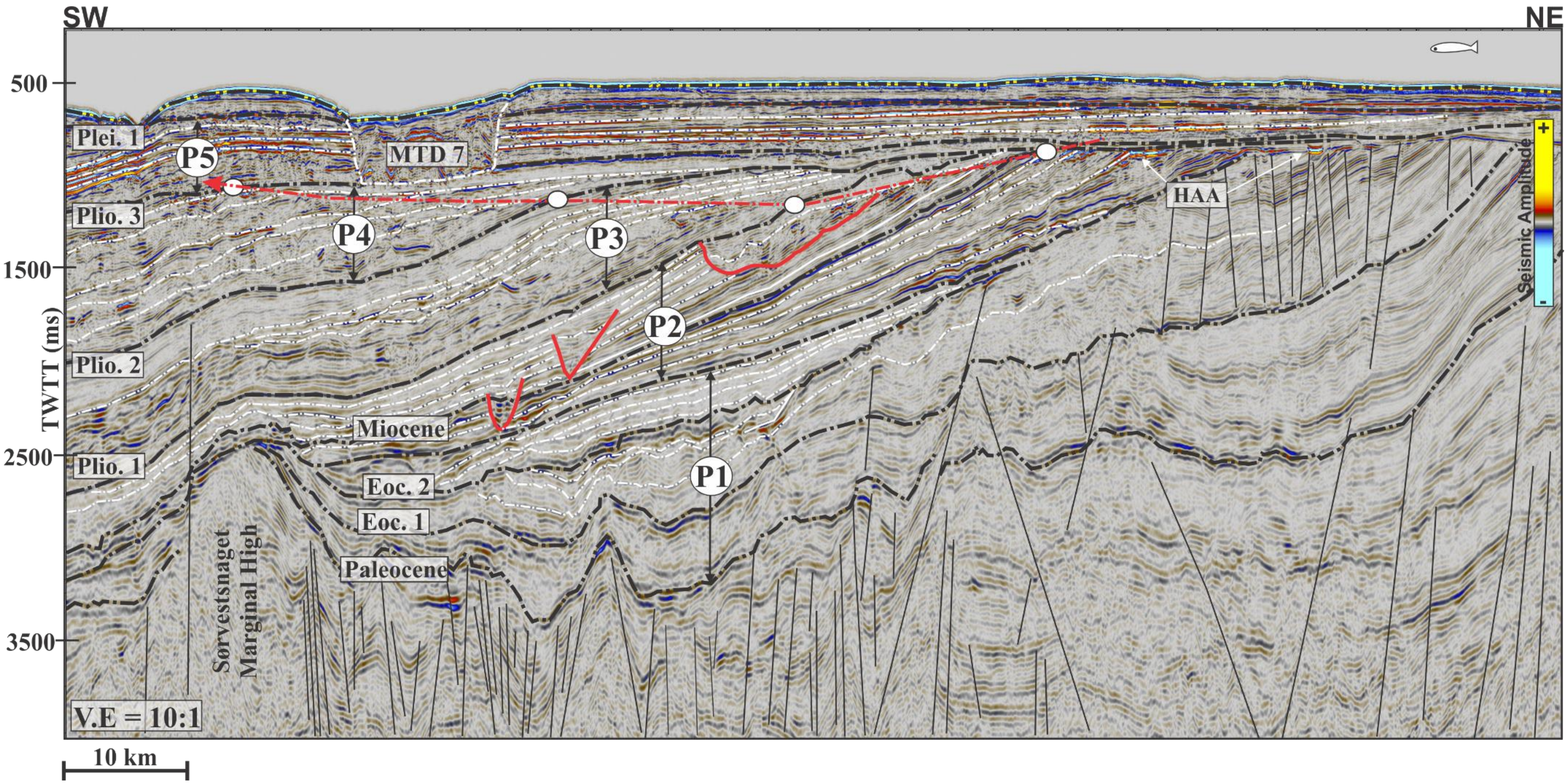

Figure 3: NE to SW seismic section through the study. The ten horizons interpreted on the seismic data include the oldest top Palaeocene unit (Kviting Formation) and the seabed reflector. The five interpreted sedimentary packages range in age from Palaeocene to Recent. The oldest package marked the upper limit of the interpreted faults. 'The Sørvestsnaget Marginal High' is a fault-bounded, salt anticline, located in the southern part of the study area. The majority of the Miocene and Eocene sediments abut against the high. Packages 2–5 consist of shelf-margin clinoforms that are several metres high and kilometres in length. *The V-shaped canyons are in red outline. The red dashed line shows the shelf edge trajectory.*

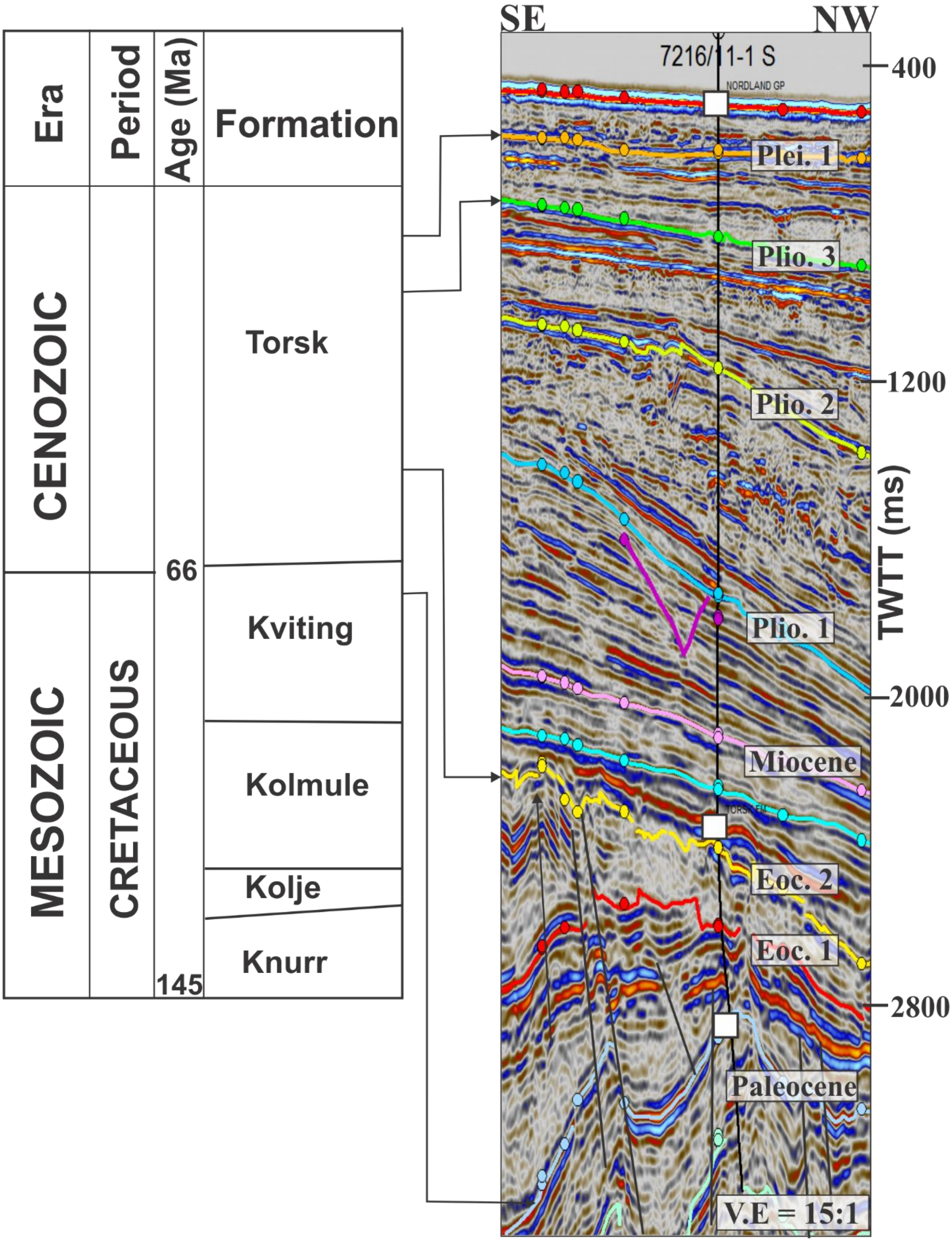

Figure 4a: Seismic-well tie showing the ages of the interpreted depositional units and their equivalent Formation tops in the borehole. See Figures 8 and 13 for petrophysical character of the MTD and canyon intersected by the borehole. *Location of the borehole is shown in Figure 1b.*

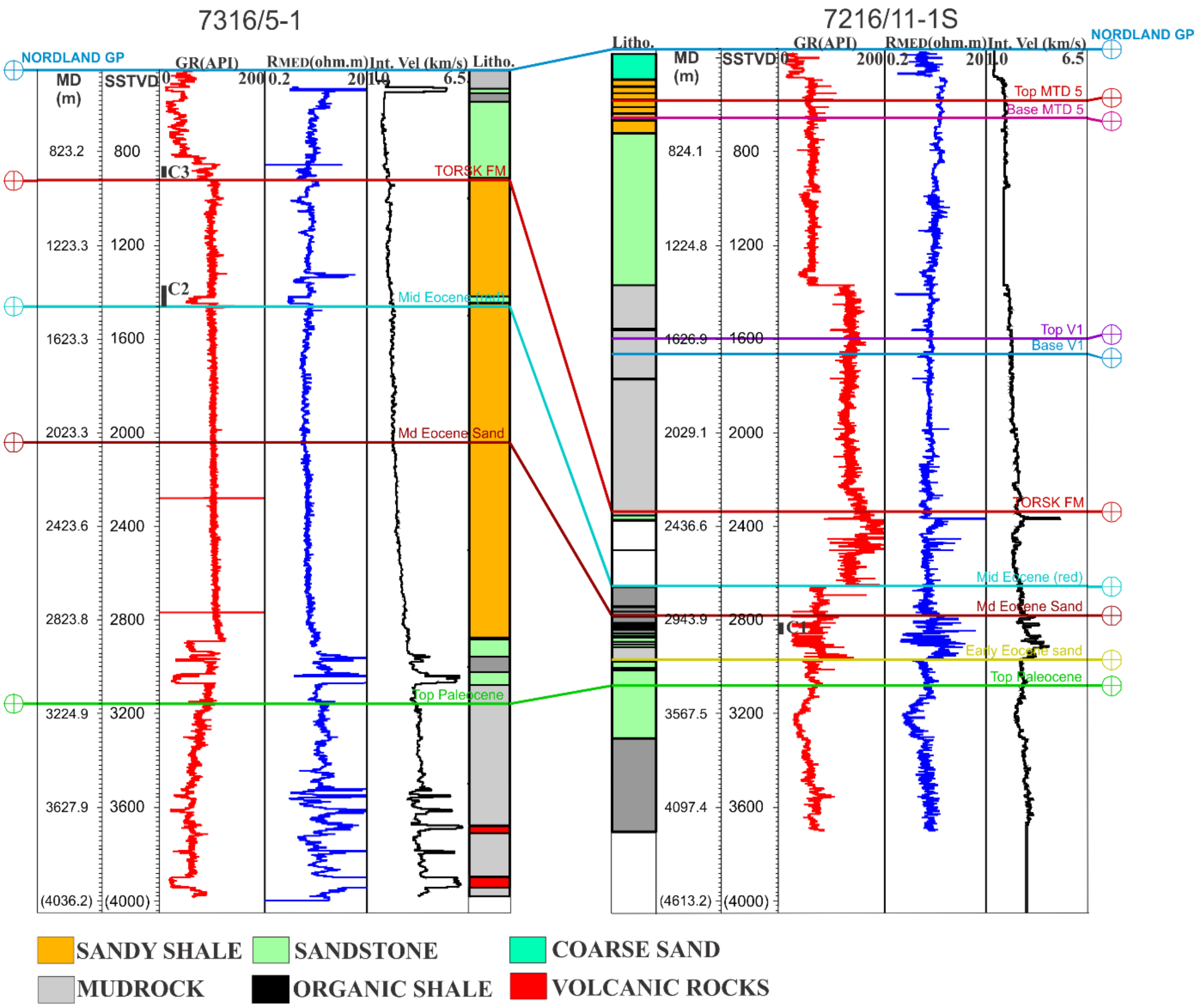

Figure 4b: Correlation panel between the two boreholes used in this work. The principal packages defined in Figure 3 are from Paleocene to Recent in age (Nordland Group). The mass-transport deposits, canyons and channels are within the Torsk Formation. *N.B: CI- (figure 5a to 5c), C2 (figure 5f and 5g) and C3 (figure 5d and 5e). Location of the borehole is shown in Figure 1b.*

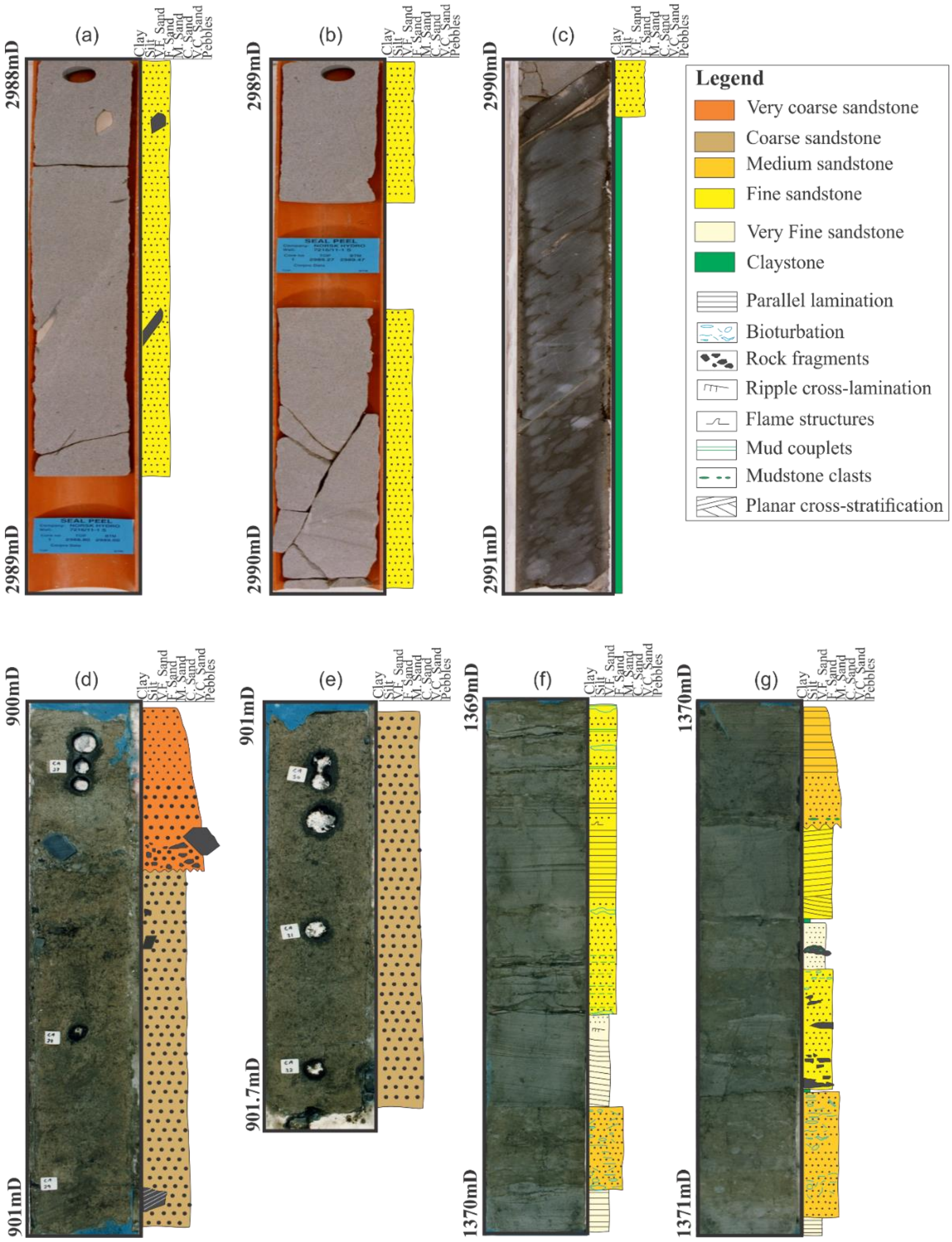

Figure 5: (a) - (c) are core photos and descriptions of Middle Eocene sandstone from borehole 7216/11-S. (d) and (e) are core photos and descriptions of Miocene sandstone from borehole 7316/5-1 (f) and (g) are core photos and descriptions of Middle Eocene sandstone from borehole 7316/5-1. Biostratigraphy analysis from Ryseth A., et al., 2003 revealed that Middle Eocene sandstone at borehole 7216/11-1S was deposited in the deep, oxygen-depleted marine depositional environment. *N.B: Core photographs courtesy NPD.*

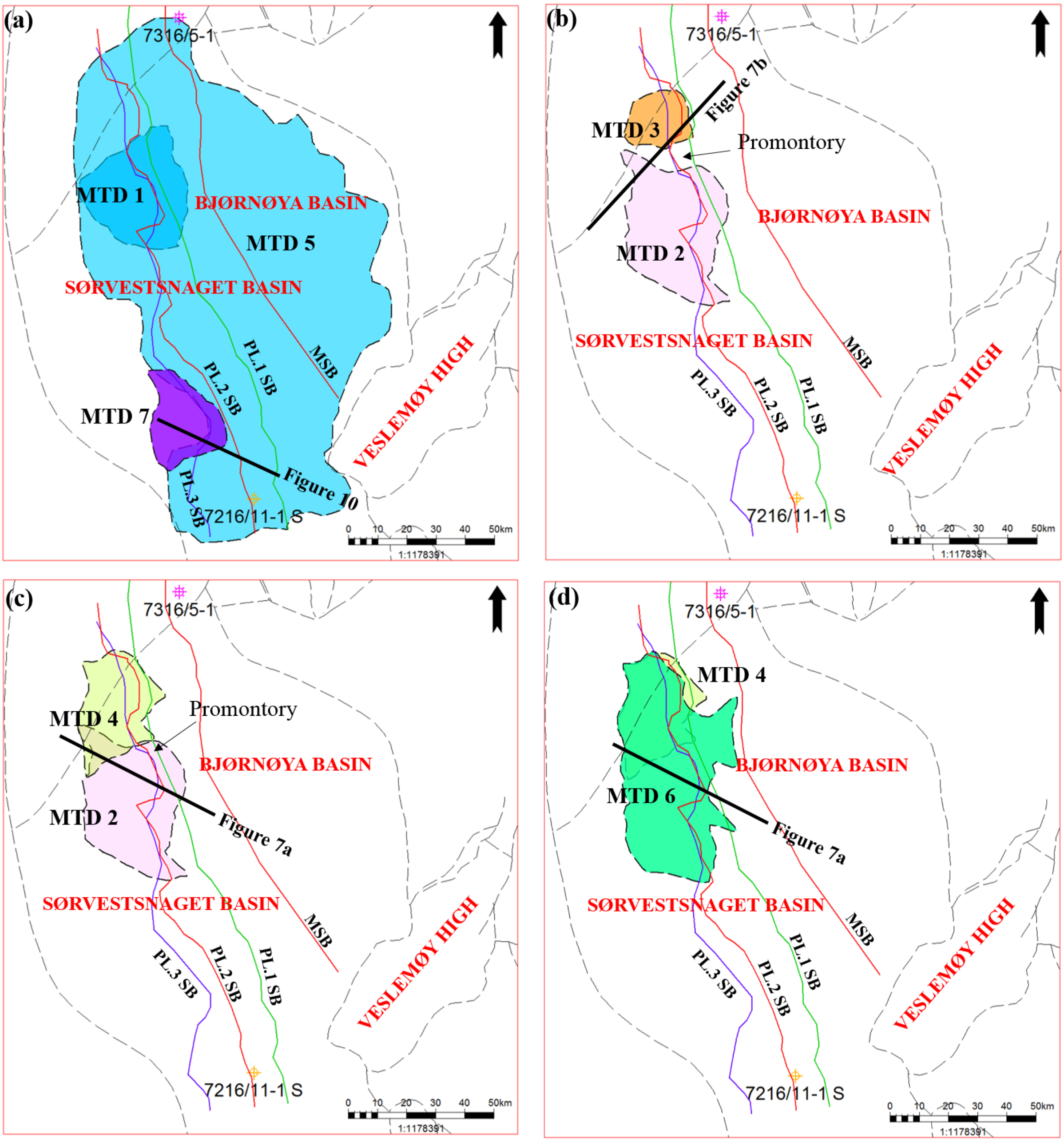

Figure 6: Plan view of the seven interpreted mass-transport deposits and the position of the shelf break from Miocene to Late Pliocene times. MTD 1 is located farther away from the Miocene shelf break position. In contrast, the other MTDs are in close proximity of the Pliocene shelf-break position except for MTD 5, which extends over the shelf into slope. (a) MTD 1, 5 and 7 (b) MTD 2 and 3, also shown in the figure is an E-W oriented promontory that separated MTD 2 from MTD 3 (c) MTD 2and 4. A minor promontory also separates the two MTDs and (d) MTD 4 and 6. *N.B: MSB- Miocene Shelf Break, PL.1- Pliocene 1 Shelf Break, PL.2- Pliocene 2 Shelf Break, and PL.3- Pliocene 3 Shelf Break. The grey dash line represents regional fault complexes.*

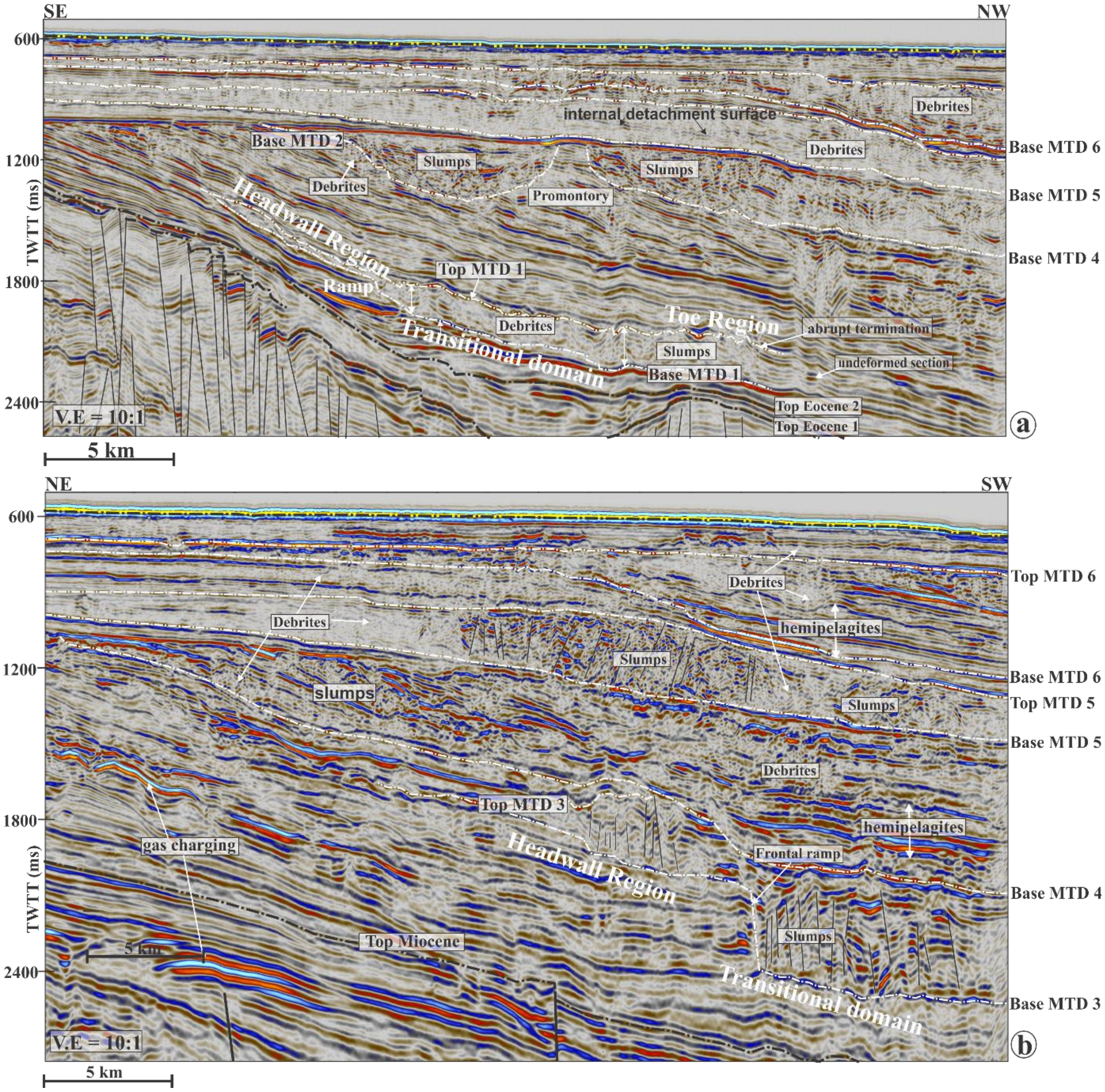

Figure 7: Seismic section through some of the MTDs, which are described as follows a) MTD 1 and 5 are homogeneous facies likened to debrites on seismic sections. The headwall region of MTD 1 records extended units, which gradually grade into slump seismic facies toward the toe region. MTDs 2, 4 and 6 are heterogeneous seismic facies; and (b) MTD 5 grades from homogeneous facies in the shelf area to very slumpy mass at the shelf break. Both MTDs 4 and 6 are characterised by a continuous and vertical stack of high-amplitude reflectors (hemipelagites) interbedded with chaotic units (debrites) at the southern part of the study area. Specifically, MTDs 1 and 3 show a series of extensional faults that sequentially cut further down dip. A frontal ramp separates the faults from the headwall region of MTD 3. *See Figure 6 for location of the seismic sections.*

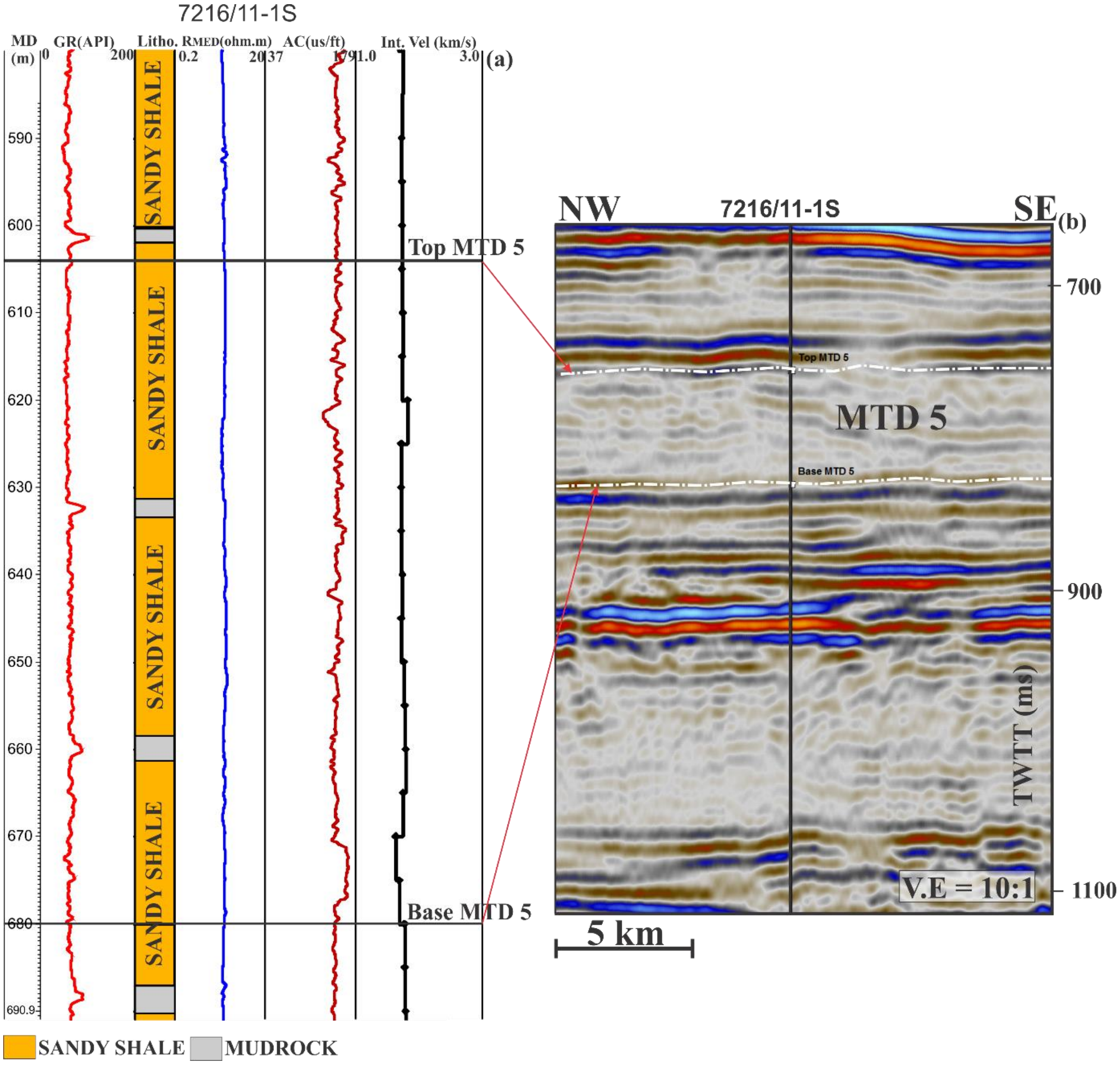

Figure 8: a) Petrophysical property of MTD 5 from borehole 7216/11-1S. The MTD is characterised by sandy shales with thin beds of mudrock, a sonic interval transit time of about 160 us/ft and a resistivity of less than 12 ohm.m. (b) Seismic section showing the well path and the time equivalent of the interval marked in (a).

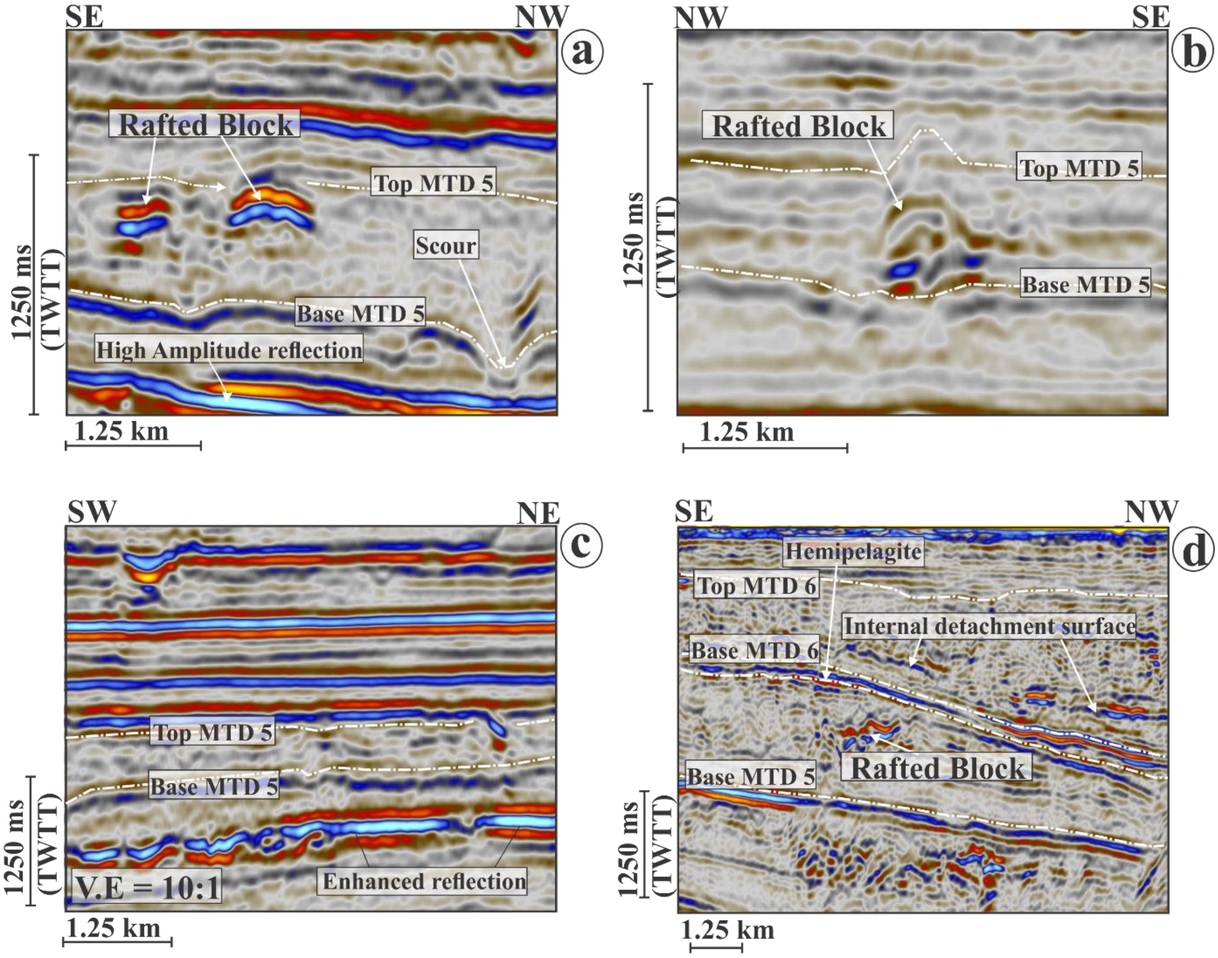

Figure 9: Internal architecture of MTDs 5 and 6 revealed features such as: (a) High-amplitude rafted blocks within homogeneous chaotic mass. The erosional groove shown at the base of MTD 5 is about 700 m wide (b) Example of rafted block from the study area. The block is about 800 ms (TWTT) high (c) Enhanced reflection underlying some of the MTDs is suggestive of the presence of gas beneath their basal shear surfaces and (d) Rafted blocks at the position of the shelf break and several continuous high reflectors within MTD 6 indicative of an internal detachment surface.

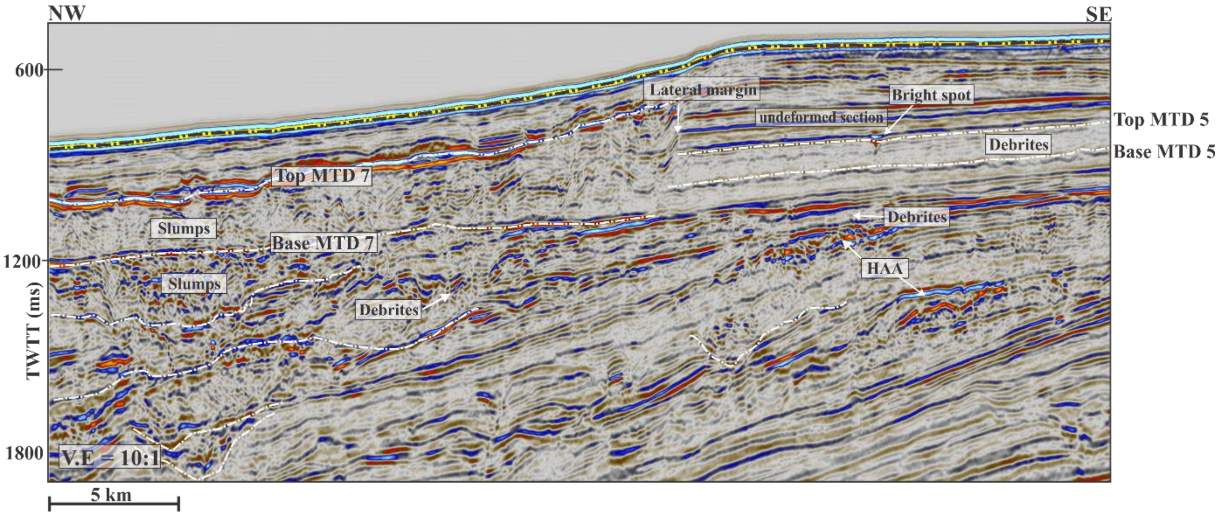

Figure 10: Lateral margin of MTD 7 and several channels infilled with slumps in the study area. In addition, several fluid-related high-amplitude anomalies are close to the interpreted MTDs. *See Figure 6 for location of the seismic section.*

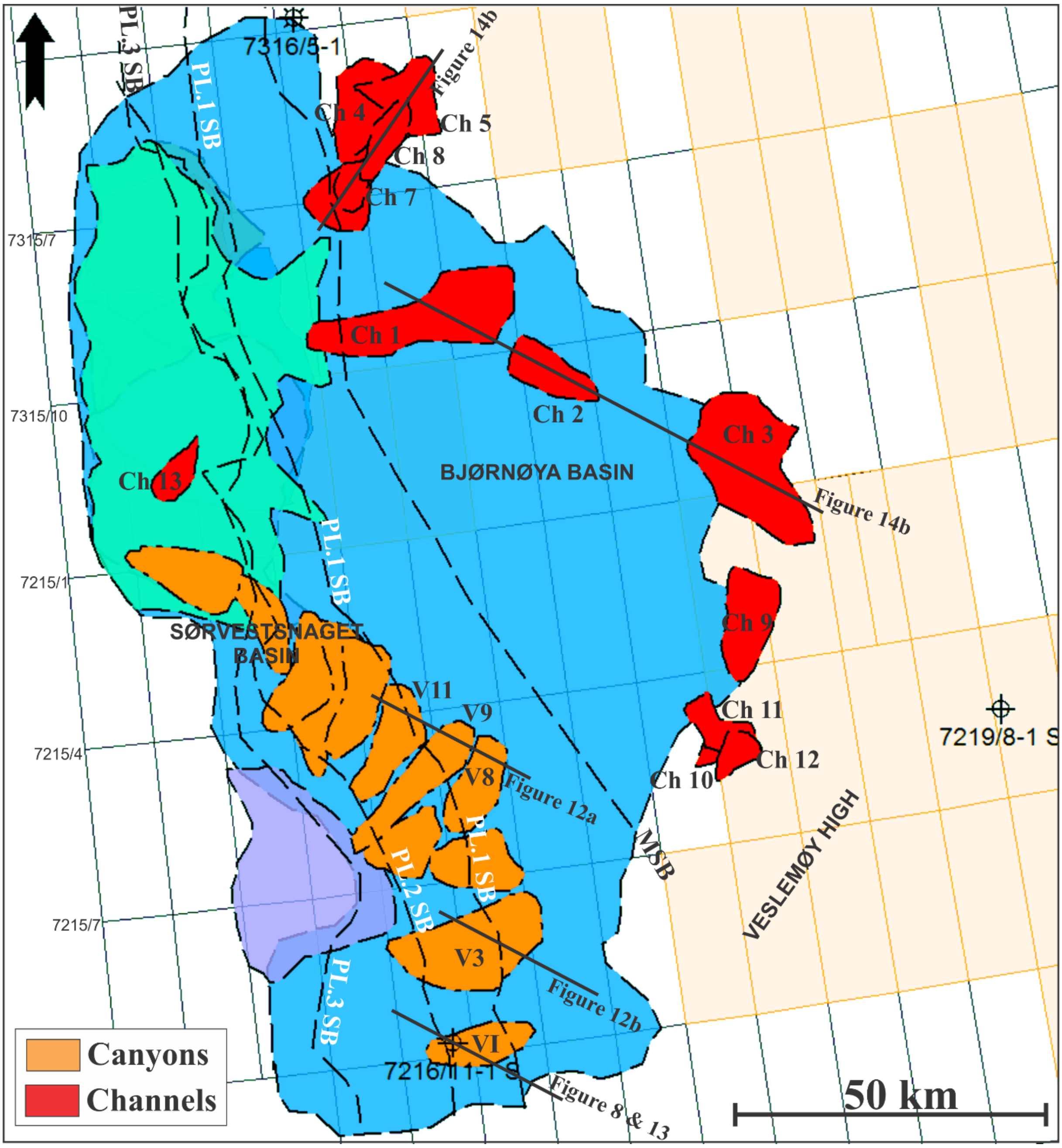

Figure 11: Map showing the distribution of the MTDs, submarine channels and V-shaped canyons interpreted in the study area. The V-shaped canyons are generally oriented in the NE-SW direction as against the multiple trend exhibited by the submarine channels. *N.B: MSB- Miocene Shelf Break, PL.1- Pliocene 1 Shelf Break, PL.2- Pliocene 2 Shelf Break, and PL.3- Pliocene 3 Shelf Break. The other colored polygons are the MTDs.*

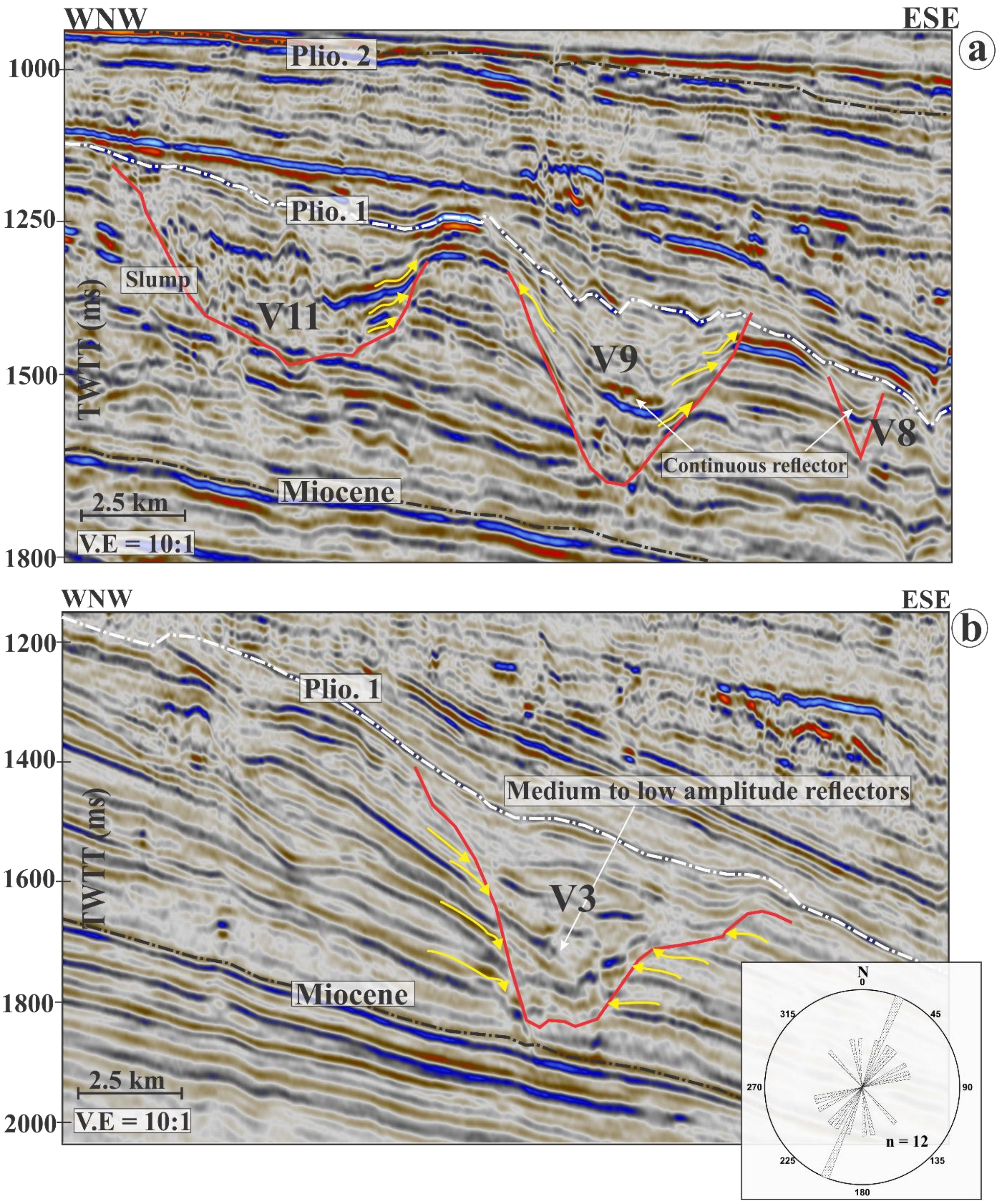

Figure 12: Evidence for subaqueous erosion in the study area includes: (a) v-Shaped canyons characterized by chaotic reflectors; and (b) v-shaped canyons containing low to moderate amplitude reflectors. The interpreted v-shaped canyons in the study area are within Package 2. The rose diagram shows the orientation of all the v-shaped canyons. *See Figure 11 for location of the seismic sections.*

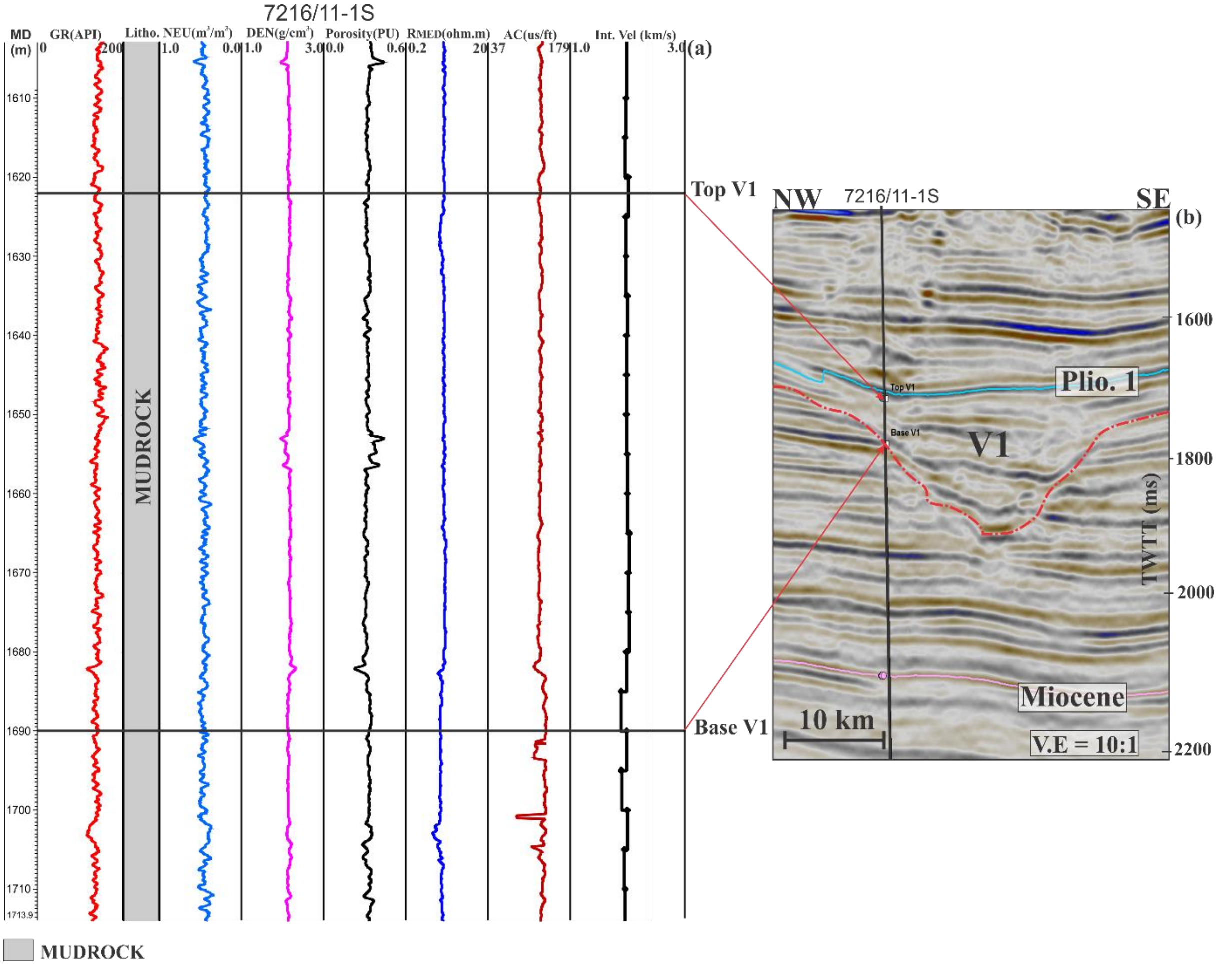

Figure 13: (a) The NW edge of canyon V1 from borehole 7216/11-1S. The unit is characterised by mudrock in the borehole (b) Seismic section showing the well path and the time equivalent of the interval marked in (a)

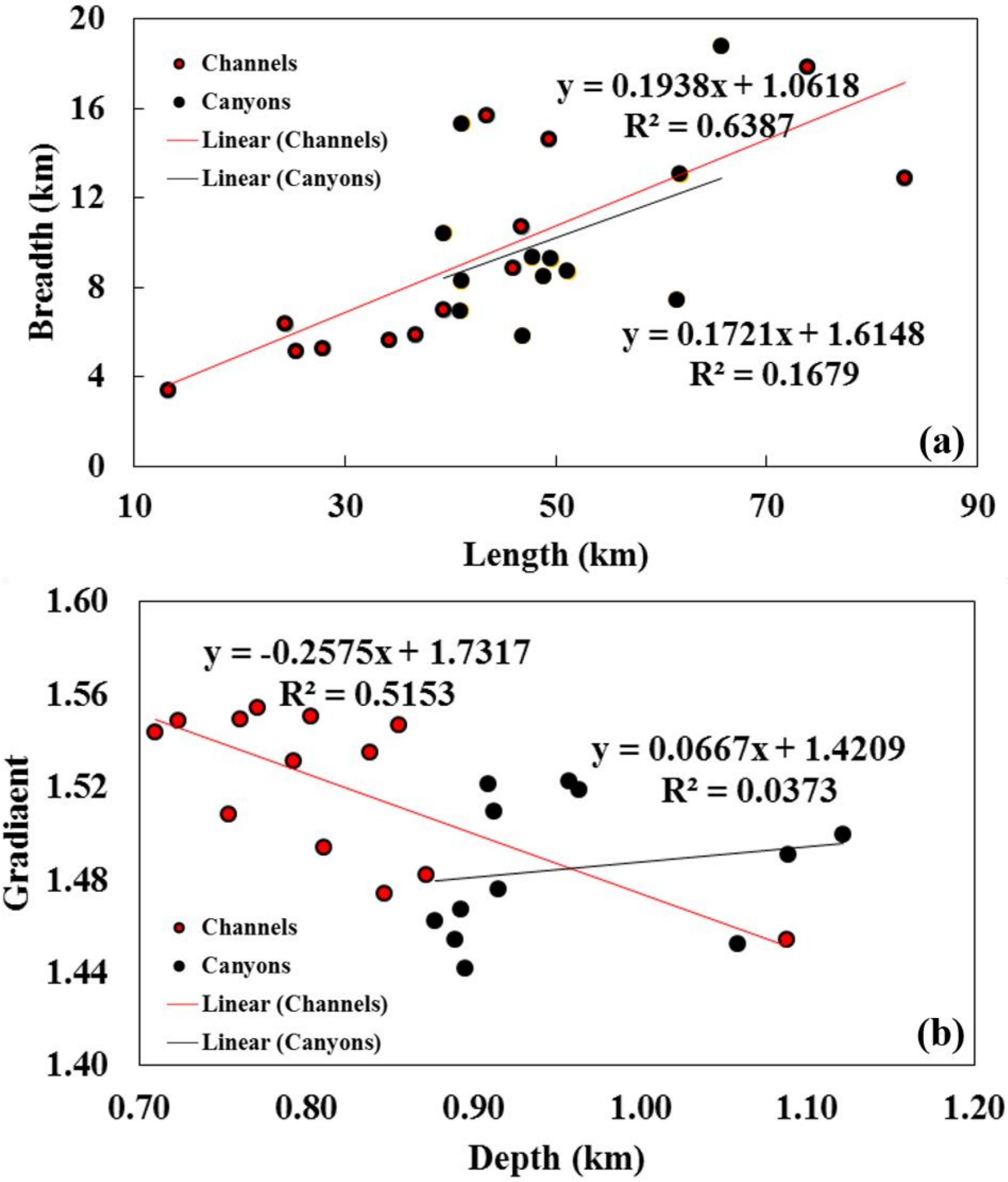

Figure 14: (a) Plot of breadth against the length of the submarine channels and canyons. The canyons positive correlation between their breadth and length with the coefficient of correlation reaching up to 0.6. On the other hand, there is low correlation between the breadth and length of the submarine channels (b) Plot of gradient versus depth/height channels and canyons in the study area.

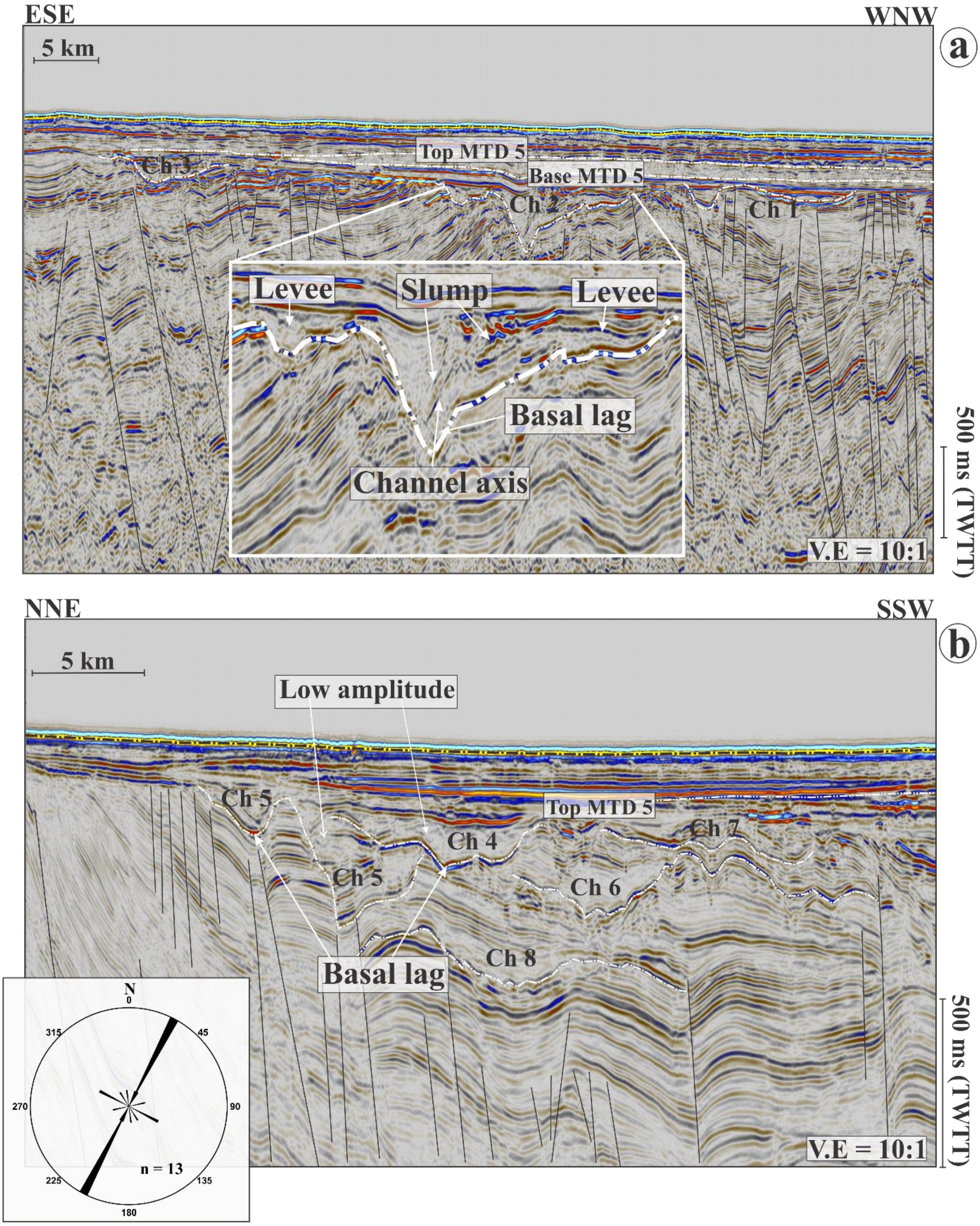

Figure 15: (a) Section through some of the submarine channels shows that the majority of them are located beneath MTD 5. Ch 2 is an example of an isolated channel; (b) submarine channels in the western part of the study area displayed complex lateral and vertical stacking. The channels show a repeated cutting and filling pattern that is characteristic of turbidites channels. In addition, the channels incised into the substrate, thereby eroding the tips of the most of the faults. The rose diagram shows the orientation of all the channels. *See Figure 11 for location of the seismic sections.*

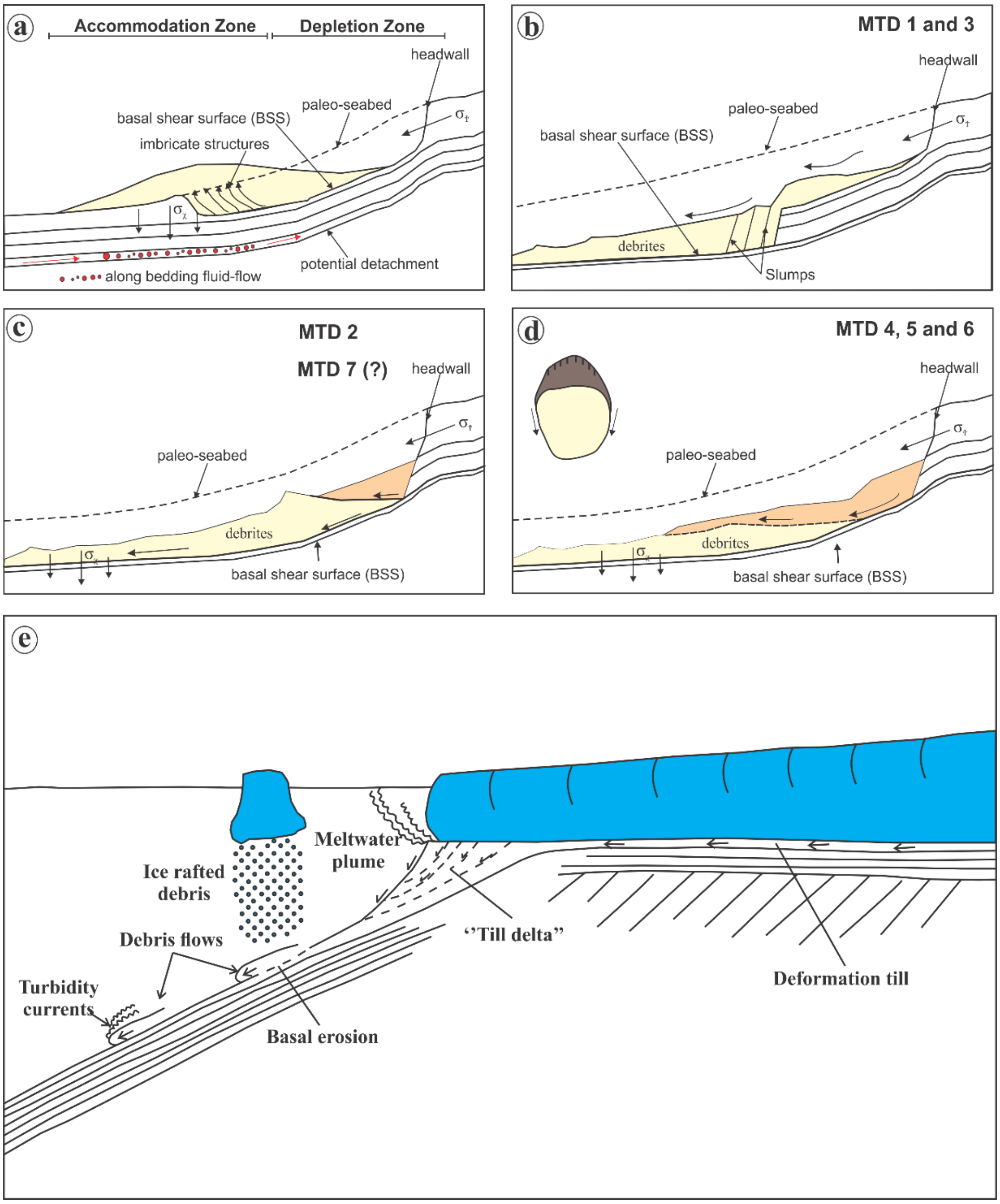

Figure 16: Conceptual model depicting the mode of propagation or mechanism for mass wasting or slope failure (Dykstra, 2005). (a) The removal of sediment from the headwall region causes a decrease in the lithostatic stress in the orientations shown by the tension arrows (σ_τ), while deposition of the MTD at the toe region causes an increase in the vertical stress (σ_χ). (b) Progressive failure occurs where a series of failures sequentially cut further downdip. Mass-transport essentially involves down-slope movement of sediments; (c) Retrogressive failure involves a series of failures that sequentially knick further headward, eventually stopping at the final headwall; (d) Whole-body failure involves an initial movement throughout all of the failing mass at the same time, after which the mass may become internally deformed. *In the boxes are listed examples of MTDs failing through each of the methods; and* (e) Schematic model showing the main sedimentary processes on the shelf break and upper slope during the presence of the ice sheet at the shelf break (from Vorren and Laberg, 1997).

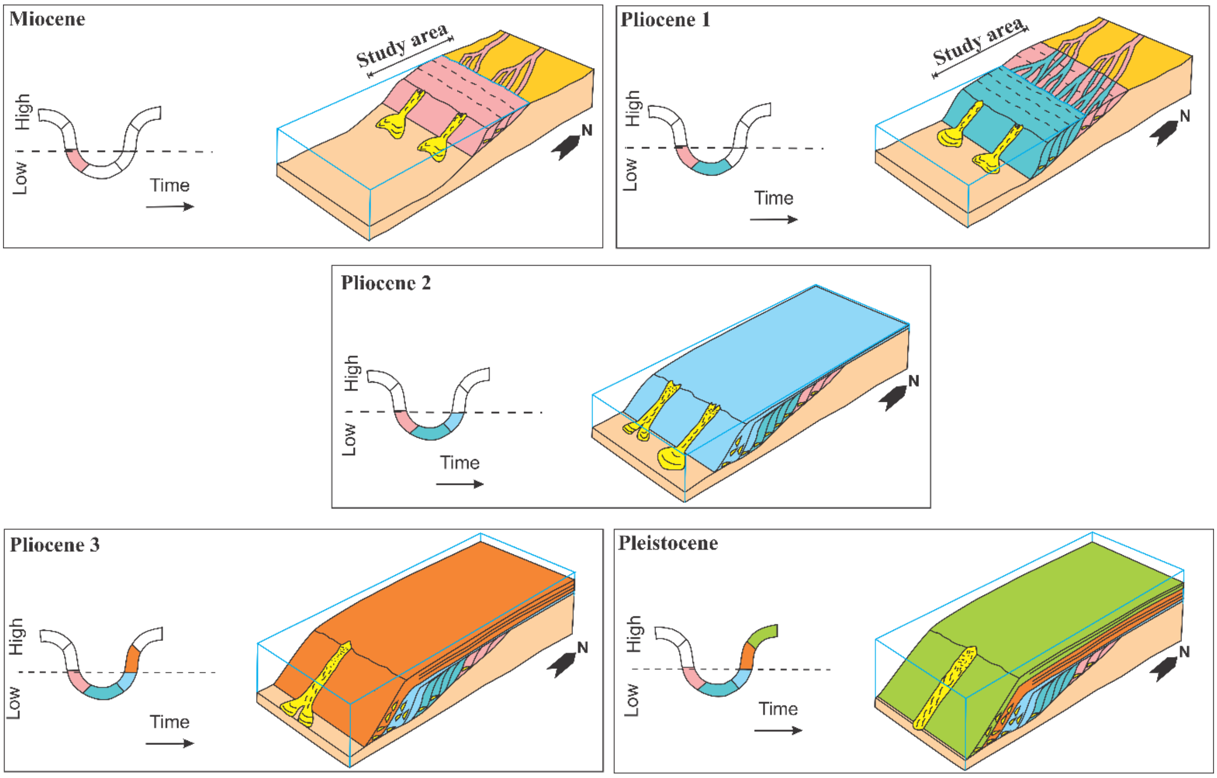

Figure 17: Block diagrams showing the evolution of the shelf and slope in the study area. There is a general westward migration of the shelf-edge from the Miocene times to the present day. The margin has witnessed increasing sea-level conditions since mid-Pliocene to Pleistocene times. The maximum fall in sea level was during the beginning of the Pliocene. Inferred sediment source or provenance is to the northern part of the study area in Stappen High.